SCATTERING AT LARGE MOMENTUM AND ENERGY TRANSFER:

APPLICATION TO NEUTRON SCATTERING ON LIQUID HELIUM

A THESIS

Presented to

The Faculty of the Division of Graduate

Studies and Research

By

Leonard Julius Rodriguez

In Partial Fulfillment

of the Requirements for the Degree

Doctor of Philosophy in the School of Physics

Georgia Institute of Technology

August, 1973

SCATTERING AT LARGE MOMENTUM AND ENERGY TRANSFER:

APPLICATION TO NEUTRON SCATTERING ON LIQUID HELIUM

Approved:

H. A. Gersch, Chairman

M. R. Flannery

M. B. Sledd

Date approved by Chairman: *16 Oct 1973*

ACKNOWLEDGMENTS

The close association of a student with his thesis adviser can erode the esteem that the student initially has for the adviser. This author can truthfully state that the reverse has occurred during his work with Dr. H. A. Gersch. The author's recognition of Dr. Gersch's excellence as a teacher and researcher has constantly increased.

Dr. M. B. Sledd performed a very extensive review of this work. His generously contributed effort healed the damage initially inflicted by the author on the gentle art of communication. The author wishes to acknowledge the effort expanded by Dr. M. R. Flannery in his review of this dissertation. Dr. I. R. Gatland and Dr. Sledd deserve thanks for their advice on mathematical details associated with this work.

On a more cryptic note, thanks to Jean for assuming responsibilities and giving the author the gift of time.

TABLE OF CONTENTS

       λ-transition and Bose-Einstein Condensation
       Neutron Scattering and Bose-Einstein Condensation

       Description of Thermal Neutron Scattering
          Experiments
       Experiment Performed by Mook, Scherm, and
          Wilkinson

       Qualitative Discussion of the Effect of
          Interactions
       Formalism for Inclusion of Final-State
          Interactions

       Discussion of the Formal Results
       Evaluation of Final-State Effects
       Extraction of Helium Liquid Properties from Data
       Final-State Effects on the Non-Condensate

TABLE OF CONTENTS (Continued)

LIST OF TABLES

LIST OF ILLUSTRATIONS

SUMMARY

A new approximation to the dynamic structure factor $S(k,\omega)$ is developed for large values of k. The approximation is intended to be used to describe inelastic nuclear scattering of thermal neutrons from a target of spinless particles of a single isotope. The approximation has the correct limit for large momentum transfer k, the impulse approximation. It is calculable in practice if the single-particle momentum distribution, the off-diagonal two-particle density matrix, and the two-body interaction potential of the target particles are known.

The approximation, which partially incorporates the effect of final-state interactions, is evaluated for a liquid ^{4}He target for momentum transfers of 14.3 $\mathring{A}^{-1}$, 28.6 $\mathring{A}^{-1}$, and 53.2 $\mathring{A}^{-1}$. The experimental results of Mook, Scherm, and Wilkinson for the scattering of neutrons from superfluid and normal liquid helium are analyzed in terms of (A) a modified impulse approximation which includes final-state corrections only in the condensate contribution to the scattering and (B) the new approximation which includes some final-state effects in both the condensate and non-condensate contributions to the scattering. These calculations substantiate a previous empirical assessment of the condensate portion of the scattering (this assessment yielded a condensate fraction of .024 ± .01) and suggest that certain barely discernible features in the experimental scattering data are real structure in the condensate contribution to the scattering. These

features appear to be attributable to the structure of the liquid
and the interaction potential of the helium atoms. Other helium
properties deduced from the data at $1.2^\circ K$ and $4.2^\circ K$ are: the
single-particle momentum distribution, the one-particle off-diagonal
density matrix, and the mean kinetic energy of the helium atoms. The
results for the single-particle momentum distribution indicate a
preferential occupation of the states with momentum of approximately
.7 $\overset{\circ}{A}{}^{-1}$. This feature is an entirely new result.

CHAPTER I

INTRODUCTION

λ-transition and Bose-Einstein Condensation

Liquid helium at temperatures below 2.18°K exhibits many interesting properties; for example, the heat conductivity becomes immeasurably large. A drastic change, such as the one which occurs in liquid helium at 2.18°K, indicates that the liquid has undergone a phase transition. This particular phenomenon in helium is called the λ-transition and the temperature at which (under saturated vapor pressure) it occurs is referred to as the λ-point. The liquid at temperatures below the λ-point is generally called either superfluid helium or He II.

Many standard textbooks describe some of the curious phenomena associated with superfluid helium such as the fountain effect, and second sound. These phenomena are explained on a macroscopic level by the two-fluid model developed largely by Landau.[2] Understanding the transition on a microscopic level has proved somewhat more difficult and is not complete at present.

The present understanding of the nature of the λ-transition starts from the observation that naturally occurring helium is almost entirely composed of the isotope ^{4}He. For thermal energies ^{4}He has a total spin of zero. Therefore, at least on an atomic scale, liquid helium is a fluid composed of massive, spin-zero bosons. The fact that a liquid

composed of ^{3}He atoms (fermions) does not undergo a transition analogous to the λ-transition indicates that the explanation of the λ-transition must closely involve the statistical properties peculiar to bosons.

An exact solution is not known for a many-body problem which includes interactions closely resembling the interactions between helium atoms. Therefore, one is forced to make some simplifications. In the literature several different sets of simplifying assumptions have been employed to study He II on a microscopic level.[3,4] The subsequent discussion will employ one of the most drastic assumptions which appear to lead to qualitatively correct results. This assumption is that the helium-helium interactions may be ignored. Treating liquid helium as a free boson gas tentatively identifies the λ-transition as coincident with the onset of the Bose-Einstein condensation[1] as follows: The number of bosons N_i occupying the quantum state i with energy ϵ_i is

$$N_i = \frac{1}{\exp(\beta\epsilon_i + \alpha) - 1} \tag{1}$$

where $\beta = 1/(k_b T)$, k_b the Boltzmann constant, T the temperature, and α a constant to be determined from the condition that

$$N = \sum_i N_i \tag{2}$$

where N is the total number of particles. The constant α is related

to the chemical potential μ by the relation $\alpha = -\beta\mu$. To be physically
meaningful N_i must be equal to or greater than zero. This implies
that $\beta\varepsilon_i + \alpha > 0$ for all ε_i, including $\varepsilon_i = 0$. Therefore, α must be
positive.

For a macroscopic system the discrete energy levels effectively
pass into a continuum; equation (1) is replaced by

$$N(\varepsilon) = \frac{g(\varepsilon)}{\exp(\beta\varepsilon + \alpha) - 1} \qquad (3)$$

where $g(\varepsilon)$ is the density of states. The density of states for a
spin-zero free-particle system is

$$g(\varepsilon) = \frac{(2m^3)^{1/2} V \, \varepsilon^{1/2}}{2\pi^2 \, \hbar^3} \qquad (4)$$

where $\hbar$ is Planck's constant divided by 2π, m is the helium atomic
mass, and V is the normalization volume. Replacing the sum in
equation (2) by an integral and combining it with the above yields

$$N = \frac{(2m^3)^{1/2} \, V}{2\pi^2 \hbar^3} \int_0^\infty d\varepsilon \, \frac{\varepsilon^{1/2}}{\exp(\beta\varepsilon + \alpha) - 1} \qquad (5)$$

The above integral may be reduced to

$$\rho = \frac{(2m^3)^{1/2}}{2\pi^2 \hbar^3} (k_b T)^{3/2} \Gamma(\frac{3}{2}) \sum_{p=0}^{\infty} (e^{-p\alpha}/p^{3/2}) \qquad (6)$$

where ρ is the number density and Γ is the gamma function. The above equation seems to contain a paradox when applied to high densities and low temperatures. The resolution of this paradox is the Bose-Einstein condensation. To see the paradox consider a system with a fixed density at some temperature T. Equation (6) can be used to determine the value of α. Now consider a process in which the system's density is held constant while its temperature is lowered. The left-hand side, LHS, of equation (6) remains constant in such a process. The factor $(k_b T)^{3/2}$ on the right-hand side, RHS, decreases as the temperature drops. To compensate, $\Sigma(e^{-p\alpha}/p^{3/2})$ must increase; therefore, α must decrease. As noted before α must be positive. So as the temperature decreases (with the density fixed), α is forced towards its lower limit, zero. For $\alpha = 0$ equation (6) becomes

$$\rho_c = (\frac{mk_b T_c}{2\pi \hbar^2})^{3/2} (2.612) \qquad (7)$$

which seems to imply that a system composed of free bosons with a density ρ_c cannot be cooled below a critical temperature T_c or, alternatively, a system of free bosons at a temperature T_c has a maximum density ρ_c. This paradoxical behavior does not occur, as was first noted by Einstein. Its appearance comes from a mathematical

oversight. Equation (7) was obtained by setting $\alpha = 0$, but from equation (3) the occupation of the state $\varepsilon = 0$ becomes infinite in the limit as α approaches zero. This 'infinity' was not treated properly in haphazard manipulations used to obtain equation (6). A correct treatment[5] verifies the following picture: In the thermodynamic limit at any temperature above the critical temperature T_c, defined in equation (7), the occupation of any microscopic state is zero. As the temperature drops, the population of the low lying states, especially $\varepsilon = 0$, increases. At temperatures below T_c a finite fraction of the total number of particles has condensed into the single microscopic state with zero energy. This macroscopic occupation of the zero energy and momentum state will be subsequently referred to as the condensate. The non-zero momentum and energy states will be referred to as the non-condensate. The speculation that the λ-transition in real helium coincides with the onset of a Bose-Einstein condensation can be aroused by using equation (7) to calculate the temperature at which a free boson system with the density of real helium would undergo the condensation. One finds $T_c = 3.2°K$, which is only $1°K$ higher than the λ-transition.

As one would expect, the Bose-Einstein condensation has been studied with more attention to mathematical rigor than used in the above discussion.[5] Also, the connection between the λ-transition and the Bose-Einstein condensation has been demonstrated with more realistic models than the free-particle model above.[3,4]

Neutron Scattering and Bose-Einstein Condensation

It is not unreasonable to insist that a connection between
the λ-transition and the Bose-Einstein condensation be observed
experimentally before such a relationship can be considered to be
established. A preliminary step would be to observe a macroscopic
occupation of the zero momentum state in real helium below the
λ-point. In the author's opinion, this has recently been accomplished
by H. A. Mook, R. Scherm, and M. K. Wilkinson by the use of neutron
scattering with large momentum transfer.[6] The primary aim of this
work is to analyze this experiment. The actual experiment is
more fully discussed in Chapter II. The following discussion develops
the connection between the helium momentum distribution and the
neutron scattering cross section for large momentum transfer.[7]

As developed in Appendix A, the inelastic scattering cross
section for neutrons on ^{4}He liquid is given in the Born approximation
by[8]

$$\frac{d^2\sigma}{d\Omega d\epsilon_f} = \frac{\sigma_b k_f}{4\pi\hbar k_i} S(\vec{k},\omega) \tag{8}$$

where $\hbar\vec{k} = \hbar\vec{k}_i - \hbar\vec{k}_f$ is the momentum transferred to the helium, $\hbar\omega = \epsilon_i - \epsilon_f$ is the energy transfer, and σ_b is the helium-atom cross
section ($\sigma_b = 1.13$ barns).[9] The dynamic structure factor $S(k,\omega)$ is
the Fourier transform of the density-density correlation function
$S(k,t)$:

$$2\pi S(\vec{k}, \omega) = \int_{-\infty}^{\infty} dt\; e^{-i\omega t} S(\vec{k},t), \tag{9}$$

where

$$NS(\vec{k},\, t) = \sum_{j,\ell} \left\langle e^{-i\vec{k}\cdot\vec{r}_{\ell}(0)}\; e^{i\vec{k}\cdot\vec{r}_{j}(t)} \right\rangle \tag{10}$$

The average value of the time-dependent density-density correlation function in equation (10) is in general taken over a canonical ensemble in equilibrium at temperature T. Equation (10) contains the Heisenberg operator $\vec{r}_{j}(t)$ defined for all j and t by

$$\vec{r}_{j}(t) = e^{iHt/\hbar}\, \vec{r}_{j}\, e^{-iHt/\hbar} \tag{11}$$

where H is the Hamiltonian of the liquid helium. It will be useful for later work to divide the density-density correlation function into two disjoint parts, the incoherent contribution $S_{i}(\vec{k},t)$

$$NS_{i}(\vec{k},t) = \sum_{j} \left\langle e^{-i\vec{k}\cdot\vec{r}_{j}(0)}\; e^{i\vec{k}\cdot\vec{r}_{j}(t)} \right\rangle \tag{12}$$

and the coherent contribution $S_{c}(\vec{k},t)$

$$NS_c(\vec{k},t) = \sum_{\substack{j,\ell \\ j \neq \ell}} \left\langle e^{-i\vec{k}\cdot\vec{r}_\ell(0)} e^{i\vec{k}\cdot\vec{r}_j(t)} \right\rangle \quad (12)$$

By this procedure one defines the incoherent and coherent contributions to the dynamic structure factor and to the scattering.

It is not evident from examination of equation (8), (9), and (10) that there is any reasonably direct connection between the inelastic scattering cross section and the momentum distribution of the liquid helium. In general there is a direct relationship between the two only when k and ω are large. For large k and ω the helium-helium interactions may be neglected and the coherent contribution may be dropped. That the coherent contribution is small for large k may be motivated by noting that for coherent scattering to occur the position of the lth atom at t = 0, $\vec{r}_1(0)$, must be correlated with the position of the jth atom at time t, $\vec{r}_j(t)$, on a length scale $1/k$. In a liquid the distances between atoms are not well correlated over very short distances. This speculation is substantiated by the experimentally determined fact that the zeroth sum rule for $k \gtrsim 6$ Å^{-1} is exhausted by the incoherent contribution

$$\int_{-\infty}^{\infty} d\omega \, S(k,\omega) \approx 1 = \int_{-\infty}^{\infty} d\omega \, S_i(k,\omega) \quad (14)$$

That the helium-helium interactions may be neglected when

considering neutron scattering at large momentum transfers may be motivated[10] by the following crude argument: It is known experimentally that the peak of the scattering occurs at an energy loss of $\hbar\omega_p \cong \hbar^2 k^2/(2m)$ for large k, $7 \overset{\circ}{A}{}^{-1} \leqslant k \leqslant 14 \overset{\circ}{A}{}^{-1}$.   From the Heisenberg uncertainty relation $\Delta t \Delta E \geq \hbar$, with the interpretation of Δt as the neutron-helium interaction time t_{nh} and $\Delta E = \omega_p$, one has

$$t_{nh} \approx \frac{2m}{\hbar k^2} \qquad\qquad (15)$$

The other quantity of interest here is the typical time t_{hh} between helium-helium interactions in the liquid. This time may be estimated by dividing the mean free path of the helium $1/\rho\sigma$, where σ is the helium-helium total cross section $\approx 35 \ \overset{\circ}{A}{}^{2}$, by the velocity of the helium atom to which the momentum k has been imparted $v_k = \hbar k/m$; this yields

$$t_{hh} \cong m/(\rho\sigma\hbar k) \qquad\qquad (16)$$

Combining equation (15) and (16) gives

$$t_{nh} \cong (\frac{1.54}{k}) \ t_{hh} \qquad\qquad (17)$$

For $k \gg 1.54 \overset{\circ}{A}{}^{-1}$ the neutron-helium interaction time is much shorter than the helium-helium interaction time. Under these conditions, the neutron does not have enough time to "see" the helium-helium

interaction. For scattering at a sufficiently large value of momentum transfer, the liquid appears, to the neutrons, as a collection of free particles. Neglect of the coherent terms and the helium interactions leads to the impulse approximation (to the Born approximation) S^{IA}. From equation (10) and (11) the impulse approximation to the density-density correlation function is

$$NS^{IA}(\vec{k},t) = \sum_j \left\langle e^{-i\vec{k}\cdot\vec{r}_j} e^{iH_o t/\hbar} e^{i\vec{k}\cdot\vec{r}_j} e^{-iH_o t/\hbar} \right\rangle \qquad (18)$$

where $H_o = \sum_\ell p_\ell^2/(2m)$. Equation (18) may be simplified by noting

$$e^{-i\vec{k}\cdot\vec{r}_j} e^{iH_o t/\hbar} e^{i\vec{k}\cdot\vec{r}_j} = e^{i(H_o + \hbar^2 k^2/2m + \hbar\vec{k}\cdot\vec{p}_j/m)t/\hbar} \qquad (19)$$

as can be verified by comparing the time derivative of the right-hand and left-hand sides of the equation and noting the obvious equality at t=0. Inserting equation (19) into equation (18) and observing that $(H_o + \hbar^2 k^2/2m + \hbar\vec{k}\cdot p/m)$ commutes with H_o yields

$$NS^{IA}(k,t) = e^{i\omega_k t} \sum_j \left\langle e^{i\vec{k}\cdot\vec{p}_j t/m} \right\rangle \qquad (20)$$

where $\omega_k = \hbar k^2/(2m)$. The above equation may be written as a sum over momentum states by using second quantization or an equivalent procedure. The result is

$$S^{IA}(k,t) = e^{i\omega_k t} \sum_{\vec{p}} n_{\vec{p}} e^{i\vec{k}\cdot\vec{p}t/m} \qquad (21)$$

where $n_{\vec{p}}$ is the single-particle momentum distribution, the expectation value of the number of particles in the momentum state $\vec{p}$ divided by the total number of particles N. Fourier transforming equation (21) in accordance with equation (9) yields the impulse approximation to the dynamic structure factor

$$S^{IA}(\vec{k},\omega) = \sum_{\vec{p}} n_{\vec{p}} \, \delta(\omega - \frac{\hbar k^2}{2m} - \frac{\vec{k}\cdot\vec{p}}{m}) \qquad (22)$$

where δ is the Dirac delta function. For a macroscopic sample of liquid helium equation (22) becomes

$$S^{IA}(k,\omega) = n_o \delta(\omega-\omega_k) + \frac{1}{(2\pi)^3 \rho} \int dp^3 n_p \delta(\omega-\omega_k-\vec{k}\cdot\vec{p}/m) \qquad (23)$$

where n_o is the condensate fraction, that fraction of the total number of helium atoms which have undergone Bose-Einstein condensation and n_p is the non-condensate distribution. If the condensate fraction is sufficiently large and if a neutron scattering experiment could be performed at a sufficiently large momentum transfer to validate the impulse approximation, the experimenter should observe a distinct two-part scattering distribution: a sharp peak proportional to the condensate fraction superimposed in the center of a broader peak

contributed by the non-condensate. Both of these conditions appear
to be partially satisfied by the experiment being analyzed.

CHAPTER II

THERMAL NEUTRON SCATTERING EXPERIMENTS

Description of Thermal Neutron Scattering Experiments

From the discussion in the Introduction, in particular Chapter
I equation (8) and (23), it appears that one could determine if there
is a significant Bose-Einstein condensate in superfluid helium by
measuring the neutron inelastic scattering cross section from He II
at sufficiently large momentum and energy transfers. This is
correct, but practical experimental considerations make the design
of an optimum experiment difficult. These considerations force a
compromise between measurement accuracy and the size of the momentum
transfer.

To perform the envisioned measurements, one must measure the
number of neutrons with a particular energy ε_f which are scattered
from an incident beam by the He II into a small solid angle "$d\Omega$".
In addition, one must know precisely the energy transfer $\hbar\omega$ and the
momentum transfer $\hbar k$. A typical method used to obtain this information
is indicated schematically in Figure 1. A collimated, monoenergic
beam of neutrons is selected from a neutron source and directed
towards the sample, in this case He II. The degree to which the
beam is collimated and monochromatic determines the experimental
accuracy to which ε_i and $\vec{k}_i$ are known. A neutron detector is
positioned at some scattering angle θ to intercept a portion of the
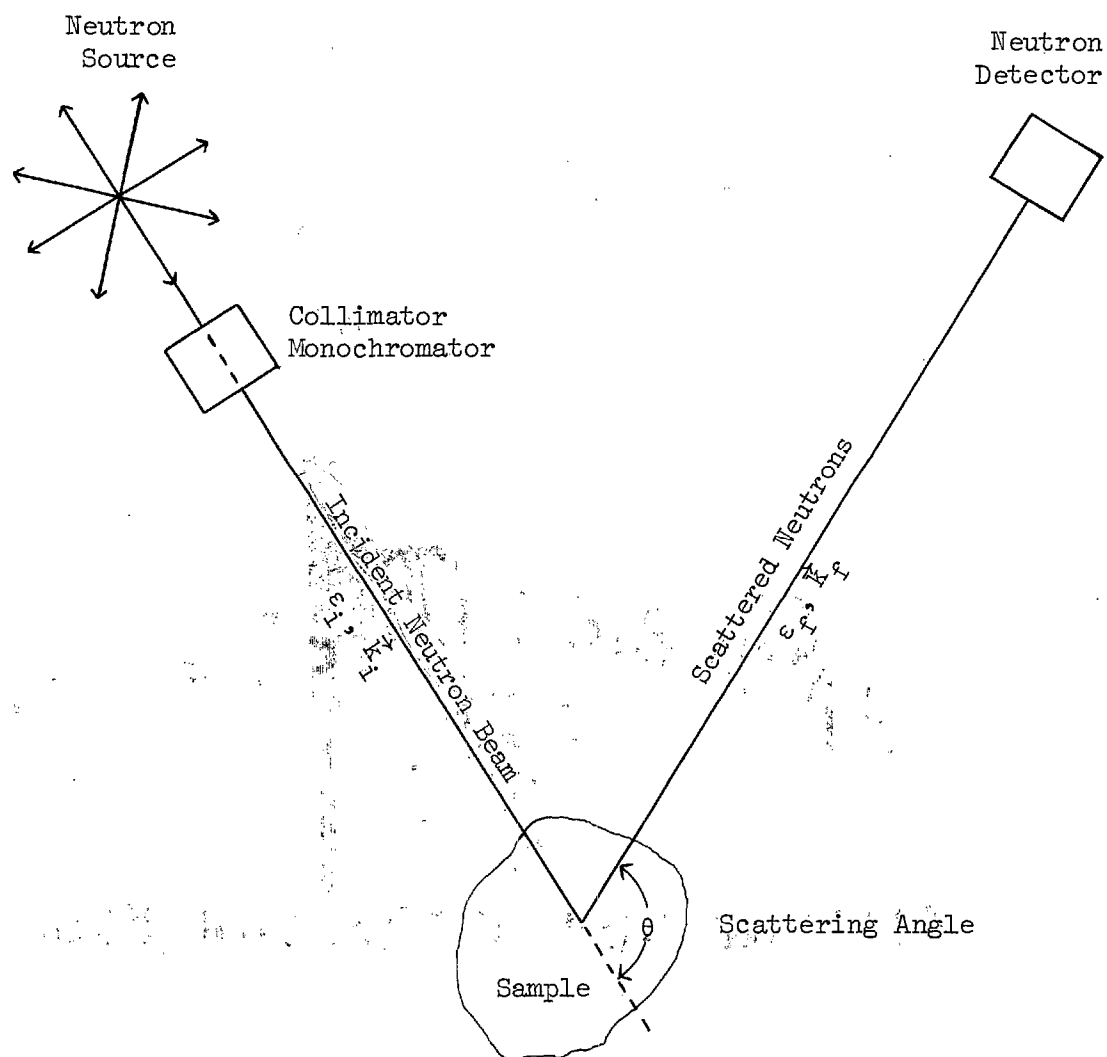
Figure 1. Schematic of a Typical Neutron Scattering Experiment.

scattered neutrons. The neutron detector counts the number of scattered neutrons which possess a particular final energy ε_f. The measured values of ε_f and θ can then be used to calculate $\vec{k}_f$ and, therefore, $\vec{k} = \vec{k}_i - \vec{k}_f$. The detector must intercept a reasonably small solid angle, since one wishes to determine the scattering into an infinitesimal solid angle $d\Omega'$. An additional requirement is that the neutrons being counted by the detector must all have been scattered from some small region in the sample. If the detector accepts scattering from a large region in the sample, the value of the scattering angle becomes imprecise, introducing errors in the values of k_f and k.[11]

A major problem in performing such an experiment can be having an insufficient number of scattered neutrons to count. The neutron source usually contains a broad spectrum of energies. Only a small fraction will have the correct energy and momentum direction to pass through the monochromator and collimator. The useable intensity may be further reduced because many material samples are relatively transparent to neutrons. In the case of interest here, the mean free path of a neutron traveling through He II can be estimated by $1/(\rho\sigma)$, where ρ is the density $\sim .022$ $\overset{\circ}{A}^{-3}$ and σ is the neutron-helium total cross section ~ 35 $\overset{\circ}{A}^2$. The result is ~ 40 cm., meaning that a typical neutron can travel through ~ 40 cm. of the liquid before it is scattered. The neutrons which do scatter from the small volume being observed scatter into essentially 4π steradians. Finally, only a small fraction enter the neutron detector to be counted.

For many applications these "inefficiencies" are overcome by using extremely high flux neutron sources. In particular, thermal neutrons available in nuclear reactors. Thermal neutrons are obtained by slowing down fission neutrons with moderators, e. g. H_2O, D_2O, and graphite. Specially designed reactors produce a flux of about 10^{19} thermal neutrons m^{-2} sec^{-1}. The neutrons approach thermal equilibrium with the moderating material. Their energy distribution is approximately represented by a Maxwell distribution corresponding to a temperature in the vicinity of $300°K$ to $400°K$. More specifically, denoting the flux of neutrons, irrespective of direction but in the wave-vector range $k_i + dk_i$, by $N(k_i)dk_i$, then

$$N(k_i) \sim \frac{n4\pi\hbar^4}{M} \left(\frac{\beta}{2\pi M}\right) k_i^3 \exp\left(-\frac{\beta\hbar^2 k_i^2}{2M}\right) \qquad (24)$$

where n is the total flux, M is the neutron mass, and $\beta = 1/(k_b T)$ (T being the temperature of the moderator). For a typical installation, the peak in the distribution occurs at a neutron energy $\varepsilon_i \sim 30meV \sim 350°K$, which corresponds to a wave-vector $k_i \sim 3.8 \, Å^{-1}$. For many applications there is an abundance of neutrons available with energies around 30 meV. The flux available decreases roughly exponentially at higher energies and wave-vectors because of the fall-off in the Maxwell distribution. This fact introduces a practical limit to the size of momentum transfer obtainable with a thermal neutron source.

In the application being discussed here, one is forced to

compromise between making the measurement at moderate momentum

transfers with an uncertainty in the applicability of the impulse

approximation (Chapter I equation (23)) and making the measurement

at large momentum transfer with large experimental errors due to

poor counting statistics.

Experiment Performed by Mook, Scherm, and Wilkinson

The following is a brief discussion of the measurement of the

inelastic scattering of neutrons by liquid helium performed by H. A.

Mook, R. Scherm, and M. K. Wilkinson. The authoritative reference

is their article in Phys. Rev. A $\underline{6}$, 2268 (1972). The balance of

the effort will be directed towards the analysis of their experi-

mental results.

The experiment was performed using a triple-axis spectrometer

at the high-flux isotope reactor located at the Oak Ridge National

Laboratory. A triple-axis spectrometer uses Bragg scattering from

a crystal to select neutrons whose energies are in a very narrow band

from the broad band of neutron energies emitted by the reactor. A

second crystal is used in the neutron detector to analyze the energy

of the scattered neutrons.

The experiment was performed with a fixed incoming neutron

energy of 182.47 ± 0.07 meV and a fixed scattering angle of 135.00

$\pm 0.02°$, which gives a typical momentum transfer of $14.3 \, Å^{-1}$.

Since there were few neutrons available at this high energy, the

counting rate at the detector was quite low, approximately one neutron

count per minute at the peak of the scattering. The low counting

rate necessitated a long counting time, approximately five months, and special attention to shielding to attain the desired accuracy.

Care was taken to minimize errors introduced by multiple reflections in the analyzing crystals. The four-dimensional resolution ellipsoid associated with the triple-axis spectrometer was calculated and measured, with good agreement. The full width at half maximum of the energy resolution was determined to be approximately 2.1 meV. The data was also corrected for changes in the volume of the resolution ellipsoid and for the changes in efficiency of the analyzing crystal and neutron counter. In the final form in which it is presented, the data is proportional to the dynamic structure factor $S(k,\omega)$ broadened by an energy resolution function with a full width at half maximum (FWHM) of 2.1 meV.

The data taken with the helium at 1.2°K (1°K below the λ-point) is shown in Figure 2. For comparison purposes, data was also taken 2°K above the λ-point at $T = 4.2$°K, shown in Figure 3. The data at 4.2°K has been corrected for the difference in the helium density between 1.2°K and 4.2°K. The data for both temperatures is presented in tabular form in Appendix B Table 7. All data has been normalized to one run, which represents about 20 minutes counting time per point.

The data taken at 1.2°K contains a subtile, but extremely interesting, feature. Approximately 5 meV above and 5 meV below the peak, there is an indication of structure in the curve. The structure is more easily observed by examining the approximate energy derivative

Figure 2. $S(k,\omega)$ for ^{4}He at 1.2°K. (Abscissa, number of neutrons scattered during a 20-minute counting time. The circles are the experimental data, Ref. 3; solid line, empirical fit $I(\omega)$. Refer to equation (2) and Table 1.)
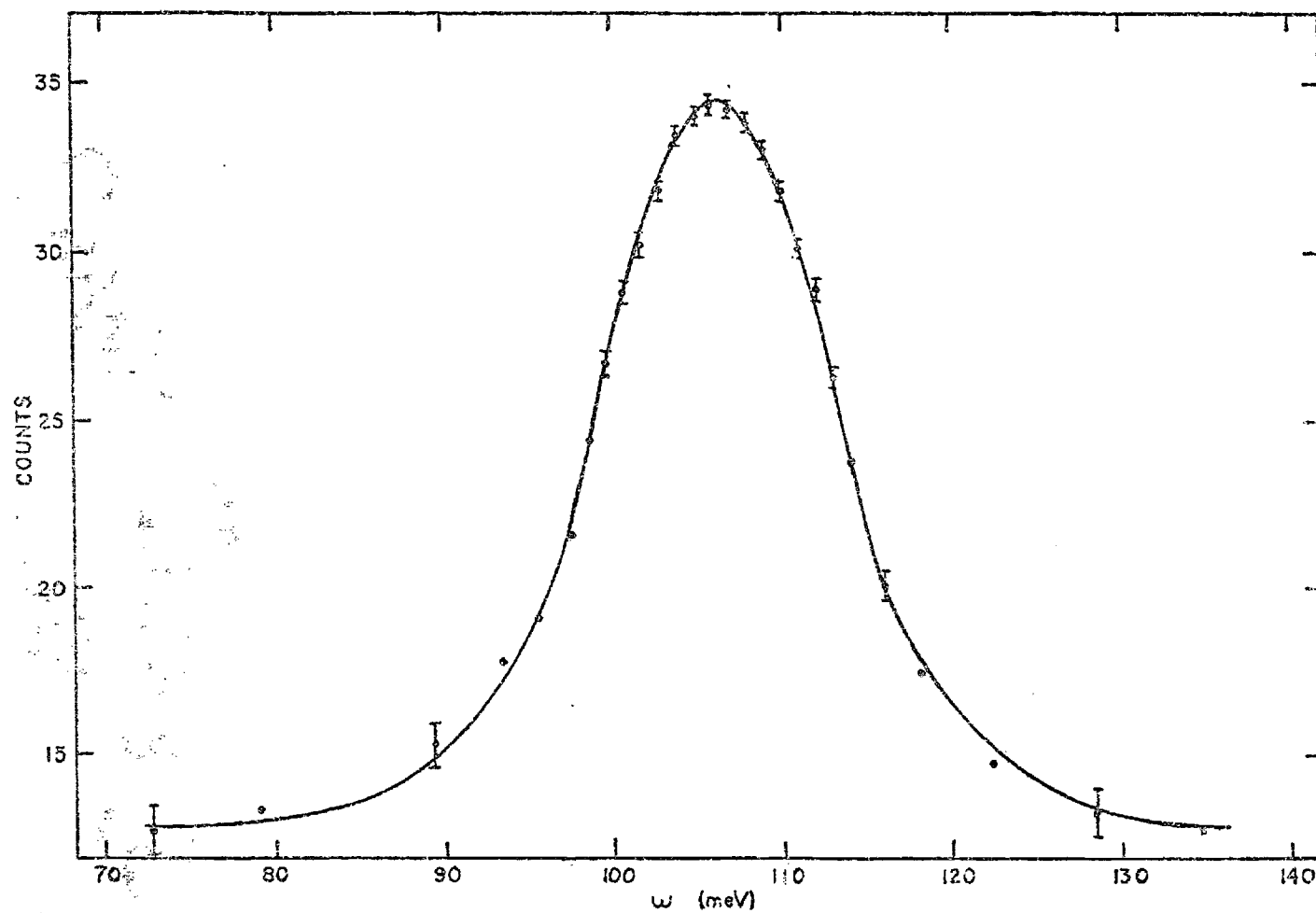
Figure 3. $S(k,\omega)$ for [4]He at 4.2°K. (Abscissa, number of neutrons scattered during a 20-minute counting time. The circles are the experimental data, Ref. 3; solid line, empirical fit $I(\omega)$. Refer to equation (2) and Table 1.)
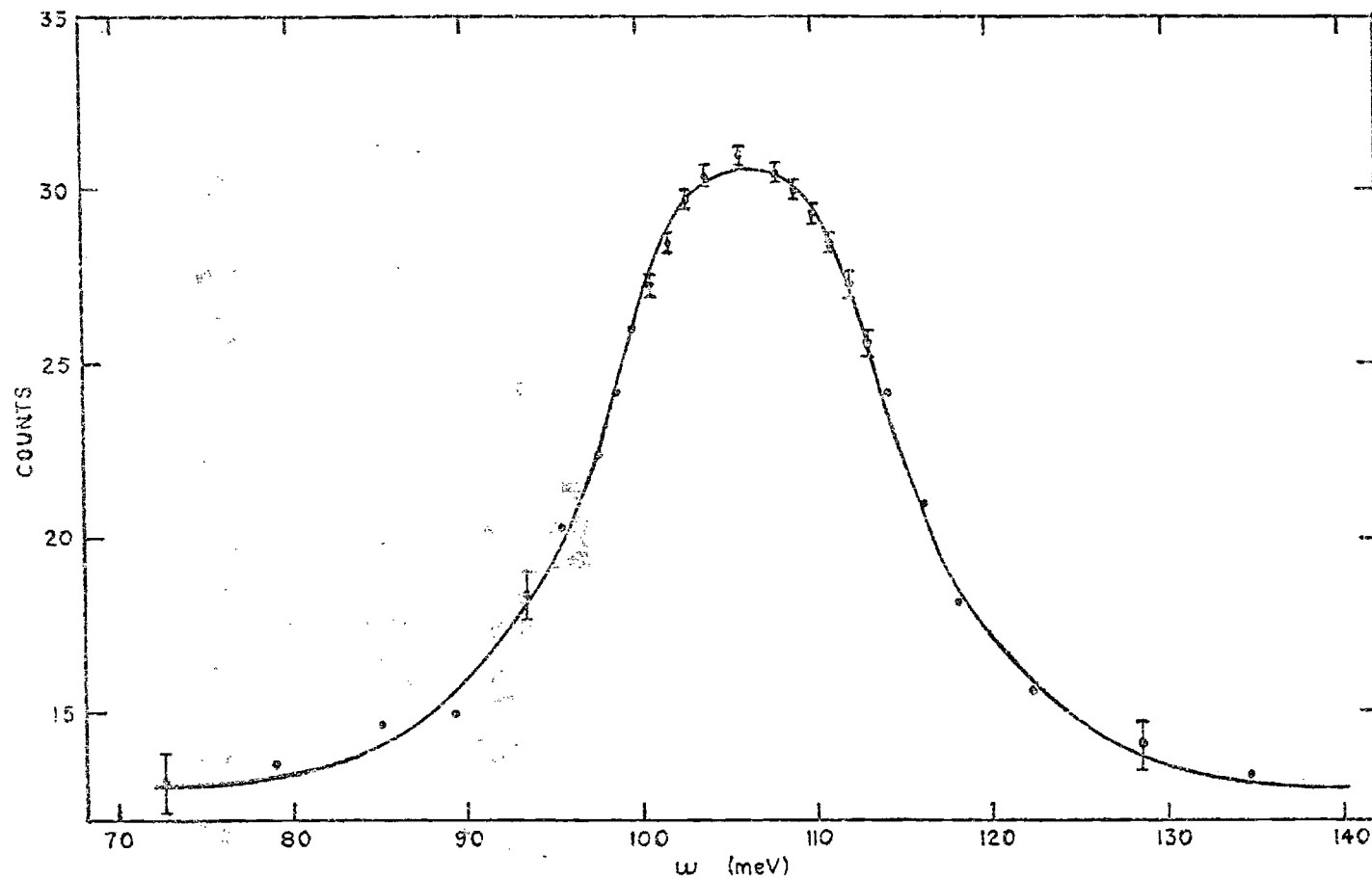
of the data; refer to Figure 3. An extremely pessimistic interpretation of the experimental errors would have to be employed to explain away this structure. Since the data at 4.2°K does not contain an analogous feature, it is tempting to attribute this structure to a Bose-Einstein condensation.

If the impulse approximation, Chapter I equation (23), is assumed to be exactly valid, one would expect the condensate contribution to the dynamic structure factor to appear as a Gaussian function with a FWHM of 2.1 meV (the delta function condensate contribution broadened by the experimental resolution function). The condensate Gaussian would be centered at $\hbar^2 k^2/(2m) \approx 106.9$ meV, superimposed on the broader non-condensate contribution. The ratio of the area under the condensate to the total area under the curve would be approximately n_o, the condensate fraction. The data will not support such an interpretation. To this author, there appear to be three possible explanations:

(1) The condensate fraction is too small at 1.2°K (possibly zero) to be measured by this experimental technique.

(2) The impulse approximation is not valid for $k = 14.3$ $Å^{-1}$.

(3) The impulse approximation is qualitatively valid at $k = 14.3$ $Å^{-1}$, but requires some modifications.

The third possibility was chosen. As to be substantiated in later calculations, the helium-helium interaction has a small effect on the rather broad non-condensate part of the scattering; therefore, the impulse approximation is valid for this part. Noting that in the
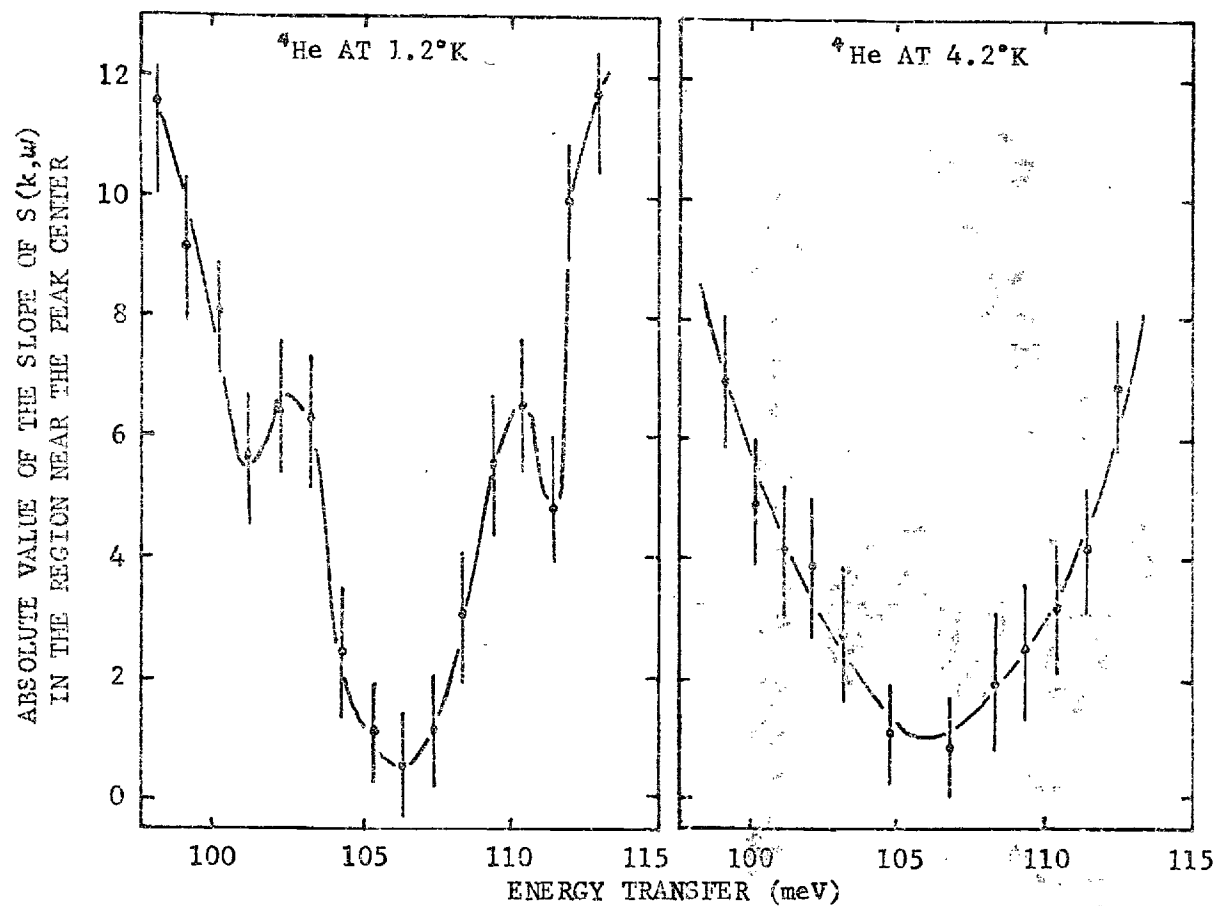
Figure 4.   Absolute Value of the Slope of $S(k,\omega)$. (Taken directly from measured data. The lines are smooth curves drawn through the data points and not the result of an analytical fit to the data.)

impulse approximation the condensate is an "infinitely narrow" delta

function, the helium-helium interactions do significantly broaden

the condensate.

Assuming the above interpretation is correct, one would expect

that the condensate would be somewhat wider than the energy resolution

function. Estimating the condensate fraction reduces itself to

resolving the dynamic structure factor into a two-part distribution

with one part taken to be the condensate contribution and the balance

the non-condensate. Mook, Scherm, Wilkinson discuss three separate

approaches to making this discrimination. The one discussed below

yields the most quantitative results.

In this technique, the data at 1.2°K and 4.2°K were subjected

to a least squares analysis. This analysis fit the energy dependence of

the measured dynamic structure factor with the function

$$I(\omega) = A_0 + A_1 e^{-(\omega-A_2)^2/A_3^2} + A_4 e^{-(\omega-A_5)^4/A_6^4} \qquad (25)$$

$$+ A_7 e^{-(\omega-A_8)^2/A_9^2}$$

where A_0, A_1 ,...,A_9 were varied to obtain the best fit with the data

taken with the helium at a temperature of 1.2°K. The data at 4.2°K

was fit by a function of the same form except that A_7 was taken as

identically zero. The values obtained for these parameters are listed

in Table 1. The first term in equation (25) was interpreted as the

Table 1. Parameters for Least Squares Fit to Data.
(Refer to equation (2). Parameters giving peak
heights are in counts per run. Parameters
representing peak widths or positions are in meV.)

Parameters	1.2°K	4.2°K
A_0	12.90	12.90
A_1	12.47	11.97
A_2	106.22	106.22
A_3	$20.76/2 \ (\ln 2)^{1/2}$	$23.28/2 \ (\ln 2)^{1/2}$
A_4	7.48	5.69
A_5	106.22	106.22
A_6	$12.82/2 \ (\ln 2)^{1/4}$	$13.48/2 \ (\ln 2)^{1/4}$
A_7	1.60	0.0
A_8	106.22	–
A_9	$4.92/2 \ (\ln 2)^{1/2}$	–

background neutron count. The sum of the second and third terms was taken as proportional to the non-condensate contribution to the dynamic structure factor. The fourth term (1.2°K data only) was identified with the condensate contribution broadened by the helium-helium interactions and the experimental resolution function. This interpretation of the data yields a condensate fraction of 2.4 ± 1 percent. This result is considerably smaller than the theoretical estimates of the condensate fraction, which range from 6 percent to 25 percent.[3,4,12,13]

CHAPTER III

THE EFFECT OF FINAL STATE INTERACTIONS
ON THERMAL NEUTRON SCATTERING

Qualitative Discussion of the Effect of Interactions

The central assumption in the Mook, Scherm, and Wilkinson

estimate of the condensate fraction is that the impulse approximation

is almost valid for a momentum transfer of 14.3 $\mathring{A}^{-1}$. In particular,

it is assumed that the impulse approximation is correct in treating

the neutron scattering as the sum of a narrow contribution from the

condensate and a broad contribution from the non-condensate, but that

the approximation is incorrect in predicting a zero width for the

condensate part. There is experimental support for parts of this

assumption. For example, the impulse approximation predicts that

the peak of the scattering will occur at an energy transfer of

$\hbar\omega = \hbar^2 k^2/(2m)$, and that the width of the scattering will be

proportional to the momentum transfer k (for experiments performed

at a constant value of k). Experiments have been performed for

momentum transfers between 0 and 14.3 $\mathring{A}^{-1}$. The experimental results

show that the impulse approximation is grossly in error for $k < 2 \mathring{A}^{-1}$,

as one would expect since the approximation is intended for large k.

For $k > 2 \mathring{A}^{-1}$, the measured peak position and width rapidly approach

the behavior predicted by the impulse approximation. Two independent

measurements[6,14] show that the actual peak of the scattering is within

1 percent of $\hbar^2 k^2/(2m)$ for $k \approx 14.3 \text{ Å}^{-1}$, the measured position in the direction of lower energy transfer. In addition, there is qualitative agreement between the shape of the measured dynamic structure fracture and the impulse approximation evaluated using a theoretical estimate of the momentum distribution.[15] There is a sufficient difference between the two to indicate that the impulse improximation or the estimate of the momentum distribution is deficient.

The assumption that the impulse approximation is "almost" correct is not indisputable. One obvious way to examine the validity of this assumption is to develop an approximation which appears to be superior to the impulse approximation for moderate values of the momentum transfer, such as 14.3 Å^{-1}. There probably is no unique program which leads to an improvement over the impulse approximation; but for this new approximation to be useful in the present context, it is subject to a severe restraint. Its evaluation must involve only simple properties of helium and helium liquid. Only a few basic microscopic properties, such as the helium-helium interaction and pair correlation function, are known with some confidence.

In the next section, an approximation is formally developed which is proposed to meet these requirements. This approximation is initiated with the bias that the impulse approximation becomes valid at sufficiently large momentum transfers. Since the impulse approximation completely neglects the helium-helium interaction, the proposed approximation will contain the interaction. The interactions,

in this context, are frequently referred to as final-state interactions.
The form of the result may be motivated by recalling the impulse
approximation

$$S^{IA}(\vec{k},\omega) = \sum_{\vec{p}} n_{\vec{p}} \, \delta(\omega - \frac{\hbar k^2}{2m} - \frac{\vec{k}\cdot\vec{p}}{m}) \tag{1}$$

and ascribing the following picture to it. The neutron strikes a
single helium particle in the target. The struck particle has a
momentum $\vec{p}$ initially. The collision is elastic and conserves the
total momentum of the neutron and helium atom. The delta function
in equation (1) is the mathematical statement that kinetic energy
and momentum are conserved in this two-body collision. This
is true only to the extent that the helium-helium interactions are
negligible. At a more modest momentum transfer, the interactions
will have some effect. Conceptually, at this lower value of k, one
could still picture the neutron as striking a single particle and
replace the remaining particles of the target by an effective
potential. The presence of this potential would remove the requirement
that the neutron-helium collision conserve momentum and allow for
inelastic processes. A momentum state $\vec{p}$ would then contribute to
the scattering not only at the precise value of the energy transfers
which satisfies $\omega - (\hbar k^2/2m) - (k \cdot p/m) = 0$, but for all ω for which
$\omega - (\hbar k^2/2m) - (k \cdot p/m)$ is small - i. e., almost elastic collisions
which approximately satisfy conservation of the neutron-particle

momentum. In mathematical terms, the delta function in equation (1) would be replaced by a finite width function $R(k, \omega - (\hbar k^2/2m)-(k \cdot p/m))$. The incoherent contribution to the dynamic structure factor would become

$$S_i(\vec{k},\omega) = \sum_{\vec{p}} n_{\vec{p}} \, R(\vec{k}, \, \omega - \frac{\hbar k^2}{2m} - \frac{\vec{k} \cdot \vec{p}}{m}) \qquad (2)$$

where the width of the function R would depend on the momentum transfer k and on the properties of the target, for example, the interaction potential of the helium particles. The width of R should decrease as k increases, approaching a delta function. Its width should also decrease if the interactions between the helium atoms were to weaken.

Formalism for Inclusion of Final-State Interactions[16]

The R function incorporates the effect of final-state interactions. Starting from the full density-density correlation function, including both coherent and incoherent terms, an expression will be developed for a slight generalization of the R function which is formally exact for all values of momentum and energy transfer. At a late stage in the development, the coherent terms will be dropped to obtain an expression for the R function for application to the liquid helium problem. This is done since the general formalism, including the coherent terms, may be applicable to other problems.

Since the intended application of this work is to neutron
scattering at large momentum and energy transfers, an attempt will
be made to motivate the formal manipulations by picturing the scatter-
ing as occurring between a neutron and the jth target particle, e. g.,
a particular helium atom in the liquid. The procedure begins by
noting that the Hamiltonians in Chapter I equation (11), which govern
the time dependence of $S(k,t)$, contain no explicit recognition that
a scattering event has changed the momentum of the jth particle. To
incorporate the modified momentum and kinetic energy of the jth
particle, the right-hand side of this equation is multiplied by
unity in the form $e^{i\vec{k}\cdot\vec{r}_j}e^{-i\vec{k}\cdot\vec{r}_j}$ from the left and then inserted
into Chapter I equation (10) (putting $\hbar = 1$):

$$NS(\vec{k},t) = \sum_{j,\ell} \left\langle e^{i\vec{k}\cdot(\vec{r}_j-\vec{r}_\ell)-i\vec{k}\cdot\vec{r}_j}e^{iHt}e^{i\vec{k}\cdot\vec{r}_j}e^{-iHt}\right\rangle \quad (3)$$

Now make use of the identity

$$e^{-i\vec{k}\cdot\vec{r}_j}e^{iHt}e^{i\vec{k}\cdot\vec{r}_j} = e^{iH't} \quad (4)$$

where

$$H' \equiv H(\vec{r}_1, \ldots, \vec{r}_N; \vec{p}_1, \ldots, \vec{p}_j + \vec{k}, \ldots, \vec{p}_N)$$
$$H' = H + \omega_k + L_j$$

with $\omega_k = k^2/2m$, $L_j = \vec{k} \cdot \vec{p}_j/m$, under the assumption that the Hamiltonian contains only kinetic energy and a velocity-independent potential. The above identify is a slight generalization of the identity displayed in Chapter I equation (19). The density-density correlation function now has the form

$$NS(\vec{k},t) = e^{i\omega_k t} \sum_{j,\ell} \left\langle e^{i\vec{k} \cdot (\vec{r}_j - \vec{r}_\ell)} e^{i(H+L_j)t} e^{-iHt} \right\rangle \tag{5}$$

In the modified Hamiltonian equation (4), the momentum lost by the neutron is explicitly transferred to the jth particle in the target. The jth particle, carrying its modified momentum $\vec{p}_j + \vec{k}$, will move in the medium of its neighbors and encounter varying potential energies. This will distort its trajectory from that of a free particle. The varying potential energy in its environment can be exhibited by using the relation

$$e^{iHt + iL_j t} = e^{iL_j t} T e^{i \int_0^t H(\vec{r}_j - \vec{v}_k t') \, dt'} \tag{6}$$

where

$$\vec{v}_k = \vec{k}/m,$$
$$H(\vec{r}_j - \vec{v}_k t') \equiv H(\vec{r}_1, \ldots, \vec{r}_j - \vec{v}_k t', \ldots, \vec{r}_N; \vec{p}_1, \ldots, \vec{p}_N) \tag{7}$$
$$H(\vec{r}_j - \vec{v}_k t') = e^{-i\vec{p}_j \cdot \vec{v}_k t'} H e^{i\vec{p}_j \cdot \vec{v}_k t'}$$

and T is the time-ordering symbol. The Hamiltonian $H(\vec{r}_j - \vec{v}_k t)$, representing the motion of the struck particle, can be rewritten in terms of the original target Hamiltonian H as

$$H(\vec{r}_j - \vec{v}_k t') = H + U_j(\vec{v}_k t') \tag{8}$$

where

$$U_j(v_k t') = \sum_{\substack{m \\ m \neq j}} V(\vec{r}_j - \vec{v}_k t', \vec{r}_m) - V(\vec{r}_j, \vec{r}_m) \tag{9}$$

under the assumption that the interaction between the target particles is adequately described by a two-body potential $V(r)$. The operator $U_j(v_k t')$ represents the change in the potential energy between the struck j^{th} particle, as it travels along a straight line trajectory with velocity $\vec{v}_k$, and the other target particles represented by m.

The density-density correlation function $S(\vec{k},t)$ is now in the form

$$NS(\vec{k},t) = e^{i\omega_k t} \tag{10}$$

$$x \sum_{j,l} \left\langle e^{-i\vec{k}\cdot(\vec{r}_j - \vec{r}_l)} e^{i\vec{p}_j \cdot \vec{v}_k t} \, T e^{iHt + i\int_0^t U_j(v_k t')dt'} e^{-iHt} \right\rangle$$

The development to this point parallels another treatment[17] of this
problem. The previous treatment proceeded by expanding the T product.
The first term in this expansion is the impulse approximation. The
subsequent incoherent terms were shown to represent corrections to
the impulse approximation ordered in increasing powers of (1/k).

As noted in a previous paragraph, the natural picture to
associate with the above procedure is of the struck particle traveling
in a straight line. This suggests that difficulties may be encountered
if the interaction between the target particles is strong for some
configurations of the particles. For example, if the interaction
contains a strong repulsive core as is characteristic of the helium-
helium interactions, the second and higher order terms in the expansion
of equation (10) have contributions from configurations in which
the struck particle can pass arbitrarily close to another particle in
the target without allowing either particle to readjust its position
to avoid a close encounter. This can be avoided by noting that the
unitary operators $e^{\pm iHt}$ in equation (10) temper the contributions
from these unphysical encounters between the struck particle and its
neighbors by allowing the particle coordinates to evolve in time.
The time evolvement of the target position coordinates can be made
more explicit by use of the identity

$$Te^{iHt + i \int_o^t U_j(v_k t')dt'} = \qquad\qquad (11)$$

$$= T e^{i \int_o^t e^{iH(t-t')} U_j(v_k t') e^{-iH(t-t')} dt'} e^{iHt}$$

which can be interpreted as a resummation of the T product in equation (10). A formal proof of this identity is given in Appendix C.[18] The exponent on the right side of equation (11) is the integral of the difference in the potential the struck particle would have encountered as a typical target particle and the potential it does encounter as the atypical struck particle

$$e^{iH(t-t')} U_j(v_k t') e^{-iH(t-t')} = \sum_m{}' \tilde{U}_{j,m}(v_k t') \qquad (12)$$

$$= \sum_m{}' V[\vec{r}_j(t-t') - \vec{v}_k t', \vec{r}_m(t-t')] - V[\vec{r}_j(t-t'), \vec{r}_m(t-t')]$$

where the term $m = j$ is deleted from the sum $\sum'$.

The function $S(\vec{k}, t)$ now has the form

$$NS(\vec{k},\ t) = e^{i\omega_k t} \qquad (13)$$

$$\times \ \sum_{j,\ell} \left\langle e^{i\vec{k}\cdot(\vec{r}_j - \vec{r}_\ell)} e^{i\vec{v}_k t \cdot \vec{p}_j} T e^{i \int_o^t dt' \sum_m{}' \tilde{U}_{j,m}(v_k t') dt'} \right\rangle$$

For a realistic many-body system, the detailed accounting for the time evolvement of all target coordinates contained in $U_{j,m}(v_k t)$ is an impossible task. In fact, it is apparent that the defining equation for $S(k,t)$, Chapter I equation (10), appears very much simpler than the result expressed by equation (13). The apparent simplicity of Chapter I equation (10) is deceptive. This becomes clear when one inserts for $\vec{r}_j(t)$ in Chapter I equation (10) an exact result which follows from the Heisenberg equations of motion:

$$i \frac{\partial \vec{r}_j(t)}{\partial t} = [\vec{r}_j(t), H] = i\vec{p}_j(t)/m;$$

$$i \frac{\partial \vec{p}_j(t)}{\partial t} = [\vec{p}_j, H] = -i \vec{\nabla}_j \sum_{\ell}{}' V(\vec{r}_j, \vec{r}_\ell)$$

These yield the equation for the time dependence of the jth target coordinate

$$\vec{r}_j(t) = \vec{r}_j(0) \tag{14}$$

$$+ \vec{p}_j(0)t/m - (1/m)\int_0^t dt'(t-t') \sum_{\ell}{}' \vec{\nabla}_j V[\vec{r}_j(t'), \vec{r}_\ell(t')]$$

inserting this expression for $\vec{r}_j(t)$ in Chapter I equation (10) and accounting for the noncommutivity of the operators in equation (14) must yield an expression equivalent to equation (13). Incidentally, it

is easy to see, by expanding Chapter II equation (10) and (13) in powers of k and comparing the terms linear in k, that (13) implies that $\vec{r}_j(t)$ is properly given by its exact value expressed in equation (14).

In equation (13) the impulse approximation still appears as an additive contribution to the dynamic structure factor. In order to obtain $S(\vec{k},\omega)$ in the form given in equation (2) and to identify the function R, a cumulant-like expansion[19] is performed. The appearance of the T product complicates the standard cumulant expansion procedure somewhat; so the details of this procedure are sketched in Appendix D. Applying this expansion yields

$$NS(\vec{k},t) = \tilde{S}^{IA}(\vec{k},t)R(\vec{k},t) \qquad (15)$$

where

$$N\tilde{S}^{IA}(\vec{k},t) = \sum_{j,l} \left\langle e^{i\vec{k}\cdot(\vec{r}_j-\vec{r}_l)} e^{i\vec{v}_k t\cdot\vec{p}_j} \right\rangle e^{i\omega_k t} \qquad (16)$$

and

$$\tilde{R}(\vec{k},t) = \exp[\omega_1 + \omega_2 + \ldots] \qquad (17)$$

where

$$\omega_1 = -e^{i\omega_k t} \qquad (18)$$

$$x \sum_{j,l,m} \left\langle e^{i\vec{k}\cdot(\vec{r}_j-\vec{r}_l)} e^{i\vec{v}_k t\cdot\vec{p}_j} \left[1-Te^{i\int_o^t \tilde{U}_{j,m}(v_k t')dt} \right] \right\rangle / S^{IA}(\vec{k},t)$$

The form of the second term, ω_2, in the exponent of equation (22) is given in Appendix D.

For systems where it is appropriate to discard the coherent contributions $j \neq l$, $\tilde{S}^{IA}(\vec{k},t)$ becomes $S^{IA}(\vec{k},t)$, the impulse approximation to the density-density correlation function

$$NS^{IA}(\vec{k},t) = \sum_{j} \left\langle e^{i\vec{v}_k t\cdot\vec{p}_j} e^{i\omega_k t} \right\rangle \qquad (19)$$

and $\tilde{R}(k,t)$ becomes

$$R(\vec{k},t) = \exp \quad -\sum_{j,m} \left\langle e^{i\vec{v}_k t\cdot\vec{p}_j} \left[1- Te^{i\int_o^t dt' U_{j,m}(\vec{v}_k t')} \right] \right\rangle / \quad (20)$$

$$\sum_{j'} \left\langle e^{i\vec{v}_k t\cdot\vec{p}_{j'}} \right\rangle + \ldots$$

Equations (19) and (20) accomplish, at least formally, the objective stated in the beginning of this chapter. When equation (15) (with

$j \neq \ell$ terms discarded) is Fourier transformed to yield the incoherent contribution to the dynamic structure factor, the result is

$$S_i(\vec{k},\omega) = \sum_{\vec{p}} n_{\vec{p}} \, R(\vec{k},\omega - \omega_k - \vec{p}\cdot\vec{v}_k) \qquad (21)$$

where the function $R(\vec{k},\omega - \omega_k - \vec{p}\cdot\vec{v}_k)$ is the Fourier transform of $R(\vec{k},t)$

$$2\pi R(\vec{k},\omega - \omega_k - \vec{p}\cdot\vec{v}_k) = \int_{-\infty}^{\infty} dt\, e^{-i(\omega - \omega_k - \vec{p}\cdot\vec{v}_k)t} R(\vec{k},t) \qquad (22)$$

Equation (21) is still an exact result for the incoherent part of $S(\vec{k},\omega)$. It is still intractable when applied to a realistic many-body system. For such systems it is necessary to apply some approximation. Our interest is in scattering at large neutron momentum transfers, and we seek an improvement over the impulse approximation, which sets the exponent $(\omega_1 \pm \omega_2 + \ldots)$ in equation (17) equal to zero for all times. The first term ω_1 in the exponent corresponds to the picture where the jth particle is struck by the neutron and then the jth particle scatters off the other particles in the target, each treated singly. The succeeding terms ω_2, ω_3, $\ldots$ in the exponent of equation (17) correspond to the scattering of the jth particle by clusters of two, three, $\ldots$ particles. One may expect that, at large momentum transfers, a meaningful correction to the

impulse approximation results from neglecting all higher-order

cumulants and retaining only the term ω_1 in the exponent of the

function $R(\vec{k},t)$ in equation (17). This approximation neglects

scattering of the jth particle by clusters of two or more target

particles.

The calculation of $R(\vec{k},t)$ is now reduced to an evaluation of

the cumulant ω_1. This appears to be a calculation of a two-body

operator until one recognizes that the appearance of $\vec{r}_j(t-t')$ and

$\vec{r}_m(t-t')$ in equation (20) leaves one with a problem of the same order

of complexity as an exact calculation of $S(\vec{k},t)$. Further progress

is made by noting that for large momentum transfers the time

evolvement of $\vec{r}_j(t-t') - \vec{v}_k t'$ is dominated by $\vec{v}_k t'$ and, therefore,

$e^{\pm iH(t-t')}$ in equation (12) may be treated cavalierly. One might,

for example, replace the time evolvement generated by the full

Hamiltonian with a time evolvement generated by an appropriate two-body

Hamiltonian describing the struck j^{th} particle and the mth particle

with which it is interacting. An even simpler, though more drastic,

approximation is obtained by completely neglecting the effect of

the factors $e^{\pm iH(t-t')}$ in giving the target particle locations a

time dependence. This corresponds to the struck particle traveling

along a straight line with the remaining particles frozen in their

t = 0 configuration, a process reminiscent of the eikonal approximation.

Neglecting the time evolvement generated by H reduces the calculation

to one in which the only information required about the target is the

one-particle off-diagonal density matrix, the two-particle off-

diagonal density matrix, and the two-body potential. This follows
from equation (20), which becomes

$$R(\vec{k},t) \cong$$ (23)

$$\exp \frac{-\sum\limits_{j,m} \left\langle e^{i\vec{v}_k \cdot \vec{p}_j t} \left[1 - e^{i \int_0^t dt' [V(\vec{r}_j - \vec{v}_k t, \vec{r}_m) - V(\vec{r}_j, \vec{r}_m)]} \right] \right\rangle}{\sum\limits_{j'} \left\langle e^{i\vec{v}_k \cdot \vec{p}_{j'} t} \right\rangle}$$

The expectation value $\left\langle e^{i\vec{v}_k \cdot \vec{p}_j t} \right\rangle$ involves only a one-body
operator and is thus reducible to a one-particle density matrix.
This reduction is performed by averaging over a single state Ψ_o
for the target system; generalization to a canonical average is
obvious. We have

$$\sum\limits_{j} \left\langle e^{i\vec{v}_k \cdot \vec{p}_j t} \right\rangle = N \left\langle e^{i\vec{v}_k \cdot \vec{p}_j t} \right\rangle = N \int \Psi_o^*(r^N) e^{i\vec{v}_k \cdot \vec{p}_j t} \Psi_o(r^N) d\tau^N \quad (24)$$

The operator $e^{i\vec{v}_k \cdot \vec{p}_j t}$ shifts the coordinate r_j appearing in $\Psi_o(\vec{r}^N)$
by the amount $v_k t$, and the integration over the coordinates $r_2, \ldots,$
r_N introduces the one-particle density matrix $\rho_1(\vec{r}_1, \vec{r}_1{}')$ defined by

$$\rho_1(\vec{r}_1, \vec{r}_1{}') = N \int \Psi_o^*(\vec{r}_1, \vec{r}_2, \ldots, \vec{r}_N) \Psi(\vec{r}_1{}', \vec{r}_2, \ldots, \vec{r}_N) d\tau_2 \ldots d\tau_N \quad (25)$$

The result is

$$\sum_j \left\langle e^{i\vec{v}_k \cdot \vec{p}_j t} \right\rangle = \int d\tau_1 \rho_1(\vec{r}_1, \vec{r}_1 + \vec{v}_k t) = \Omega' \rho_1(0, \vec{v}_k t) \qquad (26)$$

where Ω' is the volume of the target system, and we have used translational invariance of the wave function Ψ_o to obtain the last equality.

In a similar way, the expectation value in the numerator of the exponential in equation (23) involves only a sum of two-body operators and can be written in terms of a two-particle density matrix. The reduction is accomplished by writing the sum over j and m as $N(N-1)$ times the expectation value for a chosen pair, say particle 1 and 2. This term is then

$$N(N-1) \int \Psi_o^*(r^N) e^{i\vec{v}_k \cdot \vec{p}_1 t} \left[1 - e^{i\int_o^t [V(\vec{r}_1 - \vec{v}_k t', \vec{r}_2) - V(\vec{r}_1, \vec{r}_2)] dt} \right] \Psi_o(r^N) d\tau^N \qquad (27)$$

$$= N(N-1) \int \Psi_o^*(r^N) \left[1 - e^{i\int_o^t [V(\vec{r}_1 + \vec{v}_k(t-t'), \vec{r}_2) - V(\vec{r}_1 + \vec{v}_k t, \vec{r}_2)] dt'} \right] \qquad (28)$$

$$\times \quad \Psi_o(\vec{r}_1 + \vec{v}_k t, \vec{r}_2, \ldots, \vec{r}_N) d\tau^N$$

Integrating over coordinates $r_3, \ldots, r_N$ introduces the two-particle density matrix, defined by

$$\rho_2(\vec{r}_1, \vec{r}_2; \vec{r}_1{}', \vec{r}_2{}') = N(N-1) \int \psi_o^*(\vec{r}_1, \vec{r}_2, \vec{r}_3, \ldots, \vec{r}_N) \qquad (29)$$

$$x \quad \psi_o(\vec{r}_1{}', \vec{r}_2{}', \vec{r}_3, \ldots \vec{r}_N) d\tau_3 \ldots d\tau_N$$

and yields for this term the result

$$\int \rho_2(\vec{r}_1, \vec{r}_2; \vec{r}_1 + \vec{v}_k t, \vec{r}_2) \qquad (30)$$

$$x \left[1 - e^{i \int_o^t [V(\vec{r}_1 + \vec{v}_k(t-t')), \vec{r}_2) - V(\vec{r}_1 + \vec{v}_k t, \vec{r}_2)] dt'} \right] d\tau_1 d\tau_2$$

Putting $r = r_1 - r_2$ and again assuming translational invariance, this becomes

$$\Omega' \int \rho_2(\vec{r}, 0; \vec{r} + \vec{v}_k t, 0) \qquad (31)$$

$$x \left[1 - e^{i \int_o^t [V(\vec{r} + \vec{v}_k(t-t')) - V(\vec{r} + \vec{v}_k t)] dt'} \right] d\tau$$

Substituting equations (26) and (31) into equation (23) yields the function $R(\vec{k}, t)$ depending on the quantities anticapated above:

$$R(\vec{k},t) \cong \exp - \int \frac{\rho_2(\vec{r},0; \vec{r} + \vec{v}_k t, 0)}{\rho_1(0,\vec{v}_k t)} \tag{32}$$

$$\times \left[1 - e^{i \int_0^t [V(\vec{r} + \vec{v}_k(t - t')) - V(\vec{r} + \vec{v}_k t)]dt} \right] d\tau$$

Equation (32) provides a useful approximation to the effect of target atom interactions in altering the impulse approximation results for neutron scattering at high momentum and energy transfer. Two main approximations have been made to get to this result. The first consisted of the neglect of the time evolvement of the target particle coordinates (induced by the operators $e^{\pm iH(t-t')}$ in equation (13)) while interacting with the struck particle (moving with a velocity $\vec{v}_k$). The velocity $\vec{v}_k$ imparted to a target particle is much larger than a typical target atom velocity, so that for relatively soft collisions of target particles this neglect seems relatively safe. For strong, head-on collisions of the struck particle with other target particles, the readjustment of particle coordinates induced by the neglected operators $e^{\pm iH(t-t')}$ must have a large effect in preventing penetration into the hard-core region of the interaction, and here the approximation is dangerous. However, the situation encountered here is preferable to the one encountered in the expansion of the T product in equation (10). For example, if one were dealing with a Lennard-Jones potential, the quantity

$$\int_0^t U_j(v_k t') dt' = \int_0^t \sum_{\substack{m \\ m \neq j}} [V(\vec{r}_j - \vec{v}_k t', \vec{r}_m) - V(\vec{r}_j, \vec{r}_m)] dt'$$

in equation (10) and the equivalent quantity

$$\int_0^t [V(\vec{r} + \vec{v}_k(t - t')) - V(\vec{r} + \vec{v}_k t)] dt'$$

of equation (32) become undefined if the "trajectory" of the struck particle passes through the singularity of the potential. This divergence leads to an undefined expression for $S(\vec{k}, t)$ if evaluated from a finite number of terms from equation (10). In equation (32) the divergence occurs in the phase factor of an imaginary exponential and, therefore, yields a well-defined result if some sensible limiting procedure is used. A tempting speculation is that the rapid oscillatory contributions from hard collisions will be small, mimicking the more physical picture in which the remaining particles will avoid close encounters through the action of $e^{\pm iH(t-t')}$.

The second approximation contained in the final expression for $R(\vec{k}, t)$ is concerned with truncating the cumulant expansion at the term ω_1 in equation (17). The neglected terms describe correlations between two or more passive target particles during their interaction with the struck target particle. Thus, the approximate expression for $R(\vec{k}, t)$ contains multiple scatterings of the struck target particle by the remaining target particles, with each of the passive

target atoms treated independently of each other. This approximation

clearly requires that the correlation range between target atoms in

the averaging state Ψ_0 be considerably larger than the interaction

range for a pair of target particles. Although these conditions

are not completely satisfied for relatively dense systems, inclusion

of such "shadowing effects" seems inordinately difficult, requiring

adding to $R(\vec{k},t)$ terms involving three- and higher-particle density

matrices. For experimental conditions under which corrections to

the impulse approximation represented by $R(\vec{k},t)$ are relatively small,

the binary collision approximation employed here should provide a

significant description of these final-state corrections.

CHAPTER IV

ANALYSIS OF THE EXPERIMENTAL RESULTS[21]

Discussion of the Formal Results

The formalism developed in the previous chapter promises an
improvement over the impulse approximation through the partial
incorporation of final-state effects. In the impulse approximation
the helium atom which is "struck" by the neutron travels unimpeded
through the liquid. In the approximation developed in Chapter III,
the struck helium is influenced by neighboring atoms through a process
which is reminiscent of multiple single scatterings of the struck
helium by the other helium atoms in its environment. As pointed out
in that chapter, multiple single scattering is not the only process
which introduces final-state effects; there is a hierarchy of
processes in which the struck helium interacts simultaneously with
pairs, triples, quadruples, etc., of its correlated neighbors. The
decision to treat only the multiple single collision form is based
partially on the intuitive assumption that the formalism is "well-
ordered". In particular, if ignoring the scattering of the struck
helium by its neighbors (the impulse approximation) is a good first
approximation and if the inclusion of multiple single scattering
produces a small correction, then each succeeding, more complicated,
process will contribute smaller and smaller corrections.

From the results of Chapter III, the dynamic structure factor

is given by

$$S(\vec{k},\omega) = \sum_p n_p R(\vec{k}, \omega - \omega_k - \frac{\vec{v}_k \cdot \vec{p}}{\hbar}) \qquad (1)$$

where n_p is the single-particle momentum distribution (the fraction of atoms carrying momentum p), m is the helium mass, $\omega_k = \hbar k^2/(2m)$, $v_k = \hbar k/m$, and the function R

$$2\pi R(\vec{k}, \omega - \omega_k - \frac{\vec{p}\cdot\vec{v}_k}{\hbar}) = \int_{-\infty}^{\infty} dt e^{-i(\omega - \omega_k - \vec{p}\cdot\vec{v}_k/\hbar)t} R(\vec{k},t) \qquad (2)$$

incorporates final-state effects. In the multiple-single-scattering approximation, the function $R(\vec{k},t)$ may be evaluated from Chapter III equation (32). If the change of variable $y = v_k(t-t)$ is made, this equation becomes

$$R(k,t) = \exp - \int \frac{\rho_2(\vec{r}, 0; \vec{r} + \vec{v}_k t, 0)}{\rho_1(0, \vec{v}_k t)} \qquad (3)$$

$$x \left[1 - e^{i \int_0^{v_k t} [V(\vec{r} + \vec{y}) - V(\vec{r} + \vec{v}_k t)]} \right]$$

where $\rho_1(0, \vec{v}_k t)$ and $\rho_2(r, 0; r + \vec{v}_k t, 0)$ are the liquid's one-particle and two-particle off-diagonal density matrices, respectively.

In the above and subsequent equations, $\hbar$ has been set equal to unity. If the potential $V(r)$ is well-behaved, then the function $R(\vec{k},t)$ approaches unity for all time in the limit of large k.[20] In this limit, $R(k,\omega-\omega_k-\vec{p}\cdot\vec{v}_k)$ will become a delta function (refer to equation (2)) and equation (1) becomes

$$S^{IA}(\vec{k},\omega) = \sum_{p} n_p \, \delta(\omega - \omega_k - \vec{v}_1 \cdot \vec{p}) \qquad (4)$$

which is the impulse approximation derived in Chapter I (refer to equation (22) of that chapter).

Assuming there is a Bose-Einstein condensation ($n_o \neq 0$), equation (1) becomes

$$S(\vec{k},\omega) = \frac{1}{(2\pi)^3 \rho} \int dp^3 n_p R(\vec{k},\omega - \omega_k - \vec{v}_k \cdot \vec{p}) + n_o R(\vec{k}, \omega - \omega_k) \qquad (5)$$

and the impulse approximation becomes

$$S^{IA}(\vec{k},\omega) = \frac{1}{4\pi^2 \rho v_k} \int_{|\Omega|}^{\infty} dp \, p n_p + n_o \delta(\omega - \omega_k) \qquad (6)$$

where n_o is the condensate fraction, $\Omega = (\omega-\omega_k)/v_k$, and ρ is the helium number density.

A slight generalization of the impulse approximation will increase the range of momentum transfer over which it is a good approximation. This modification is the replacement of the delta function condensate contribution by the R function

$$S^{IA}(\vec{k},\omega) = \frac{1}{4\pi^2 \rho v_k} \int_{|\Omega|}^{\infty} dp \ p n_p + n_o R(k,\omega - \omega_k) \qquad (7)$$

This approximation will be useful for those values of k for which the width of the R function is narrow compared to the width of n_p, allowing the replacement of R by a delta function in the integrated term of equation (5) even though the condensate term may have measurable width. In subsequent discussion, equation (9) will be referred to as the impulse approximation. It includes the effect of final-state interactions on the condensate portion via the R function but neglects these effects in the non-condensate part.

Recalling the basic premise made in the analysis of the condensate fraction by Mook, Scherm, and Wilkinson, one can see that both equation (5) and equation (7) partially support this premise. These equations separate the dynamic structure factor into a contribution from the non-condensate, which is related to the non-condensate momentum distribution n_p with $p \neq 0$, and a contribution from the condensate $n_o R(k,\omega-\omega_k)$ which in general has a non-zero width. Two points remain to be considered. The first is the plausibility of the Gaussian condensate $A_7 \exp[-(\omega-A_8)^2/A_9^2]$ found by the least squares analysis

discussed in Chapter II. This will be examined by evaluating the theoretical estimate of the condensate contribution, represented by $n_0 R(k, \omega - \omega_k)$, for the conditions corresponding to the experiment and then comparing the results to the assumed Gaussian form for the condensate. This will be done in the next section. The second point is the plausibility of the non-condensate portion of the dynamic structure factor. If one knew the single-particle momentum distribution and the R function, this could be accomplished by evaluating the integrated term in equation (5) for the experimental conditions. Attempts have been made to evaluate the momentum distribution from first principles, but it is difficult to gauge the validity of the results. Rather than trying this approach, the data will be analyzed to determine the momentum distribution which would produce the observed dynamic structure factor. The credibility of the momentum distribution so calculated then reflects on the credibility of the assessment of the non-condensate portion of the data, at least within the framework of the approximations being used.

Evaluation of Final-State Effects

The evaluation of the R function is the central problem of this approach to the analysis of neutron scattering. $R(\vec{k}, \omega - \omega_k - \vec{v}_k \cdot \vec{p})$ evaluated for $p = 0$ is proportional to the condensate contribution to the dynamic structure factor; and, when properly convoluted with the momentum distribution (refer to equation (5)), it yields the non-condensate part. In order to evaluate the R function in a straight-forward manner, it is necessary to select forms for the helium-helium

interaction potential $V(r)$, the one-particle density matrix $\rho_1(0, \vec{v}_k t)$, and the two-particle density matrix $\rho_2(\vec{r}, 0; \vec{r} + \vec{v}_k t, 0)$.

The Lennard-Jones potential was used to represent the helium-helium interaction

$$V(r) = 4\varepsilon[(\sigma/r)^{12} - (\sigma/r)^6] \tag{8}$$

with $\varepsilon = 10.22^\circ K$ and $\sigma = 2.556 \text{ Å}^3$. The selection of the two-particle density matrix was based on the following considerations. Viewing ρ_2 as a scalar product in (N-2)-particle Fock space

$$\rho_2(\vec{r}, 0; \vec{r} + \vec{v}_k t, 0) = \left\langle \phi_0 \middle| \Psi^+(\vec{r}) \Psi^+(0) \Psi(\vec{r} + \vec{v}_k t) \Psi(0) \middle| \phi_0 \right\rangle$$

where the helium is assumed to be in the ground state ϕ_0, the Schwartz inequality yields

$$|\rho_2| \leq \left\langle \phi_0 \middle| \Psi^+(\vec{r}) \Psi^+(0) \Psi(0) \Psi(\vec{r}) \middle| \phi_0 \right\rangle^{1/2} \tag{9}$$

$$\left\langle \phi_0 \middle| \Psi^+(0) \Psi^+(\vec{r} + \vec{v}_k t) \Psi(\vec{r} + \vec{v}_k t) \Psi(0) \middle| \phi_0 \right\rangle^{1/2}$$

Assuming that the ground state can be represented by an everwhere positive wave function, ρ_2 is positive and the absolute value symbol may be removed, so that

$$\rho_2(\vec{r}, 0; \vec{r} + \vec{v}_k t, 0) \leq \rho^2 g^{1/2}(\vec{r}) g^{1/2}(\vec{r} + \vec{v}_k t) \tag{10}$$

where $g(r)$ is the pair correlation function. When $t = 0$, the inequality in equation (10) becomes an equality; therefore, one expects $\rho^2 g^{1/2}(\vec{r}) g^{1/2}(\vec{r} + \vec{v}_k t)$ to be a good approximation to ρ_2 for small values of t and all values of r.

For large values of $(\vec{r})$ and $(\vec{r} + \vec{v}_k t)$, ρ_2 should approach the Hartree-Fock approximation

$$\rho_2(\vec{r},0; \vec{r} + \vec{v}_k t,0) \cong \rho \rho_1(\vec{r}, \vec{r} + \vec{v}_k t) + \rho_1(\vec{r},0)\rho_1(0,\vec{r} + \vec{v}_k t) \qquad (11)$$

For most choices of $(\vec{r})$ and $(\vec{r} + \vec{v}_k t)$, the direct term $\rho\rho_1(\vec{r}, \vec{r} + \vec{v}_k t)$ will dominate the exchange term $\rho_1(\vec{r},0)\,\rho_1(0, \vec{r} + \vec{v}_k t)$, since $\rho_1(0,R) = \rho_1(R,0) \approx \rho n_0$ for $R \gtrsim 4\text{Å}$ (refer to Figure 10). If the exchange term is neglected, the approximation used for ρ_2 which agrees with equation (12) and (13) in their regions of applicability is

$$\rho_2(\vec{r},0; \vec{r} + \vec{v}_k t, 0) \approx \rho g^{1/2}(\vec{r}) g^{1/2}(\vec{r} + \vec{v}_k t)\,\rho_1(0, \vec{v}_k t), \qquad (12)$$

where translational invariance has been used to replace $\rho_1(\vec{r},\vec{r} + \vec{v}_k t)$ by $\rho_1(0, \vec{v}_k t)$. Estimates indicate that $g^{1/2}(r)$ is essentially zero for $r \lesssim 2\text{Å}$, then rises sharply to approach unity at $r \approx 3\text{Å}$, and exhibits rapidly damped oscillations about unity for $r \gtrsim 3\text{Å}^3$. To simplify the calculation somewhat, $g^{1/2}(r)$ and $g^{1/2}(\vec{r} + \vec{v}_k t)$ were replaced by unit step functions, yielding

$$\rho_2(\vec{r}, 0; \vec{r} + \vec{v}_k t, 0) \tag{13}$$

$$\simeq \rho \; \Theta(|\vec{r}| - r_0)\Theta(|\vec{r} + \vec{v}_k t| - r_0)\rho_1(0, \vec{v}_k t)$$

In equation (13), r_0 is treated as a parameter which may be adjusted slightly under the restriction that $\Theta(|r| - r_0)$ remain a reasonable approximation to $g^{1/2}(r)$. Since only the ratio $\rho_2(\vec{r}, 0; \vec{r} + \vec{v}_k t, 0)/\rho_1(0, \vec{v}_k t)$ appears in equation (5), the above approximation for ρ_2 removes the need to choose a form for ρ_1.

The above approximation to the two-particle density matrix, equation (13), is most appropriate for zero temperature because of the assumption that the state of the helium liquid is described by an everwhere positive wave function. The R function calculated with this approximation will be compared with data taken at a helium temperature of $1.2°K$. This assumes that taking ρ_2 to be everywhere positive at $1.2°K$ introduces an error which is not incommensurably large compared to the error introduced by the other approximations used in obtaining equation (13).

Before proceeding, it may be useful to make some comments about $R(\vec{k}, t)$. By suitable manipulations of equation (3) it may be shown that

$$R^*(\vec{k}, t) = R(\vec{k}, -t) \tag{14}$$

implying that the real part of $R(\vec{k},t)$ is an even function of t and that the imaginary part is a odd function of t. When Fourier transformed to yield $R(k, \vec{v}_k\Omega)$, the real part of $R(\vec{k},t)$ will produce the even part (in Ω) of $R(\vec{k}, v_k\Omega)$, and the imaginary part will yield the odd part of $R(\vec{k}, v_k\Omega)$. If, in turn, $R(\vec{k}, v_k\Omega)$ is convoluted with n_p in accordance with equation (3) to produce the non-condensate contribution to $S(\vec{k},\omega)$, the primary effect of the even part of $R(k, \vec{v}_k\Omega)$ will be to modify the width of the dynamic structure factor, and the main effect of the odd part will be to change the peak location from that of the impulse approximation.

Some general observations about the shape of $R(\vec{k},t)$ can be made more conveniently by considering the negative logarithm of R

$$R(k,t) \equiv e^{-E(v_k t)} \tag{15}$$

In our approximation $E(v_k t)$ is given by

$$E(v_k t) = \rho \int dr^3 \; \theta(|\vec{r}| - r_0)\theta(|\vec{r} + v_k t| - r_0) \tag{16}$$

$$x \left[1 - e^{\frac{i}{\vec{v}_k}\int_0^{\vec{v}_k t} dy[V(\vec{r} + \vec{y}) - V(\vec{r} + \vec{v}_k t)]} \right]$$

which is obtained from equation (3). A simple physical picture may be associated with mathematical operations called for in the evaluation of equation (16). In this picture a helium atom is struck by the incoming neutron at its initial position $\vec{r}$. The struck helium then travels along a straight line trajectory from its initial position $\vec{r}$ to its final position $(\vec{r} + \vec{v}_k t)$ at a velocity $\vec{v}_k$ and in a time t. During its "flight", the struck helium interacts with a single helium located at the origin of the coordinate system. This interaction will be loosely referred to as scattering of the struck helium. A particular choice of initial position $\vec{r}$ will be referred to as a configuration.

First note that the Lennard-Jones potential $V(r')$ used in this calculation becomes highly repulsive as r' decreases below r_0 (more precisely for $r \lesssim \sigma = 2.556$ Å, but $r_0 \approx \sigma$). The potential is weakly attractive for $r_0 \leq r \leq R$, where R is some distance beyond which the potential is insignificantly small for the purpose of this calculation (in actual computations R was taken to be 8 Å though its value depends somewhat on k and t). Also, note that the unit step functions in equation (18) remove all configurations for which the initial and/or final position is within the core defined by a sphere of radius r_0 about the origin of the coordinate system. This means that for small $v_k t$, $v_k t \ll 2r_0$, the hard repulsive part of the potential does not contribute to the scattering. The value of $E(v_k t)$ is therefore small, being determined by the weak attractive part of the potential.

For the repulsive part of the potential to contribute, the path of the struck particle from $\vec{r}$ to $(\vec{r} + \vec{v}_k t)$ must pass completely through the core of radius r_0. As $v_k t$ approaches $2r_0$, these configurations begin to contribute and soon to provide the dominant portion of the value of $E(v_k t)$. For large $v_k t$, as shown in Appendix E, $E(v_k t)$ is dominated by a term linear in $v_k t$

$$E(v_k t) \rightarrow (\frac{\rho \sigma_\tau}{2} + i4\pi \frac{\rho}{k} \, Re \, f(k, k))v_k t + C' \qquad (17)$$

where σ_τ is the total helium-helium cross section and $Re \, f_e(k,k)$ is the real part of the forward scattering amplitude, both evaluated in the eikonal approximation, and C' is bounded. The term $\rho \sigma_\tau/2$ is just twice the reciprocal of a simple estimate of the mean free path. Therefore, this term is reminiscent of the results of phenomonological arguments which yield $1/\rho \sigma_\tau$ as an estimate of the width of the condensate portion of the scattering. It should be noted that the factor 1/2 and the additive real part of C' will make the width of $R(k,t)$ significantly different from the estimate $1/\rho \sigma_\tau$.

The value of $E(v_k t)$[22] was determined by numerical integration of equation (16) for selected values of k, t, and r_0; the results for the real part of $E(v_k t)$ are shown in Figure 5; the imaginary part in Figure 6.

The real part of equation (16) appears to be well behaved with small computational error. A smooth curve has been drawn through
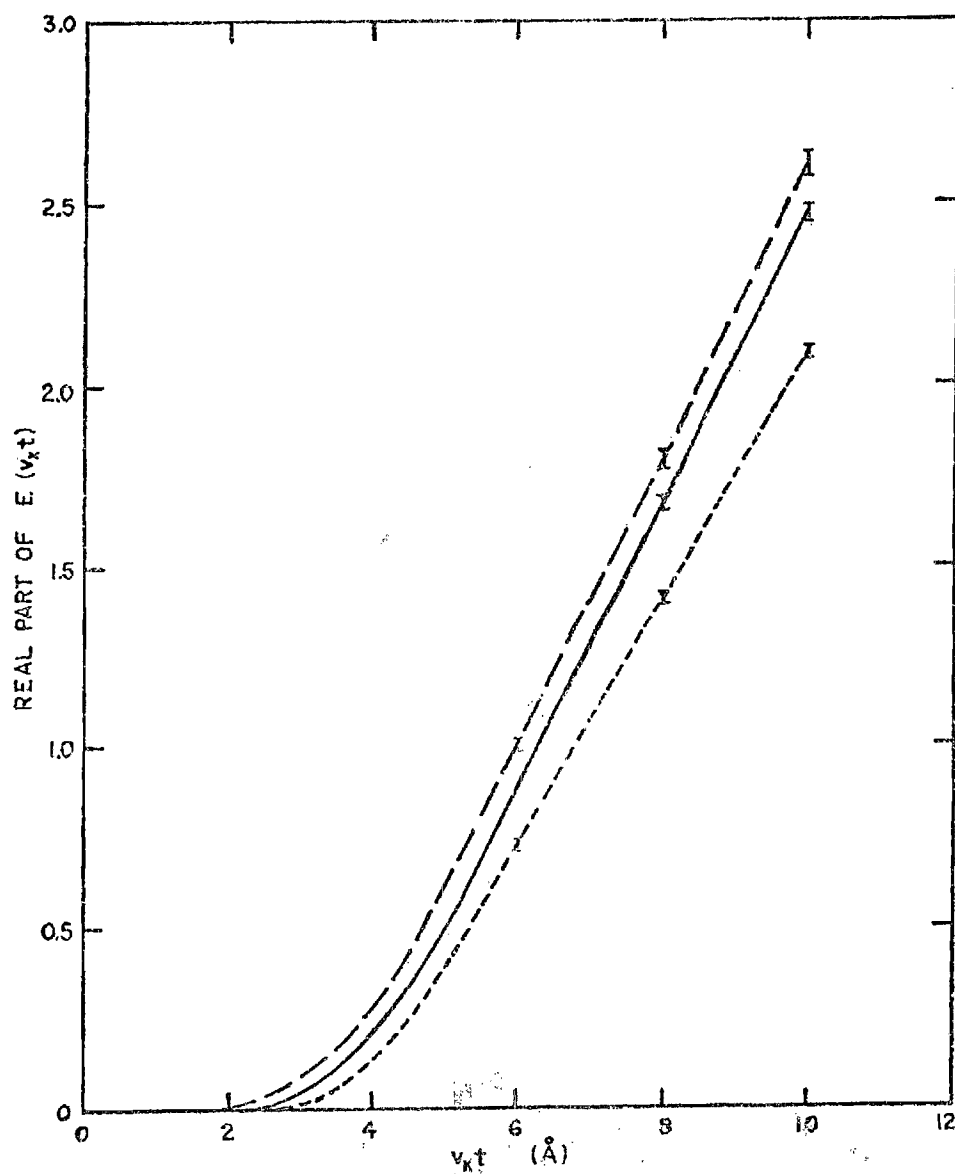
Figure 5. Real Part of $E(v_k t)$. (The solid line evaluated with $k = 14.3$ $Å^{-1}$ and $r_0 = 2.5$ Å; long-dashed line, $k = 14.3$ $Å^{-1}$ and $r_0 = 2.4$ Å; short-dashed line, $k = 28.6$ $Å^{-1}$ and $r_0 = 2.5$ Å. Errors indicated where significant.)
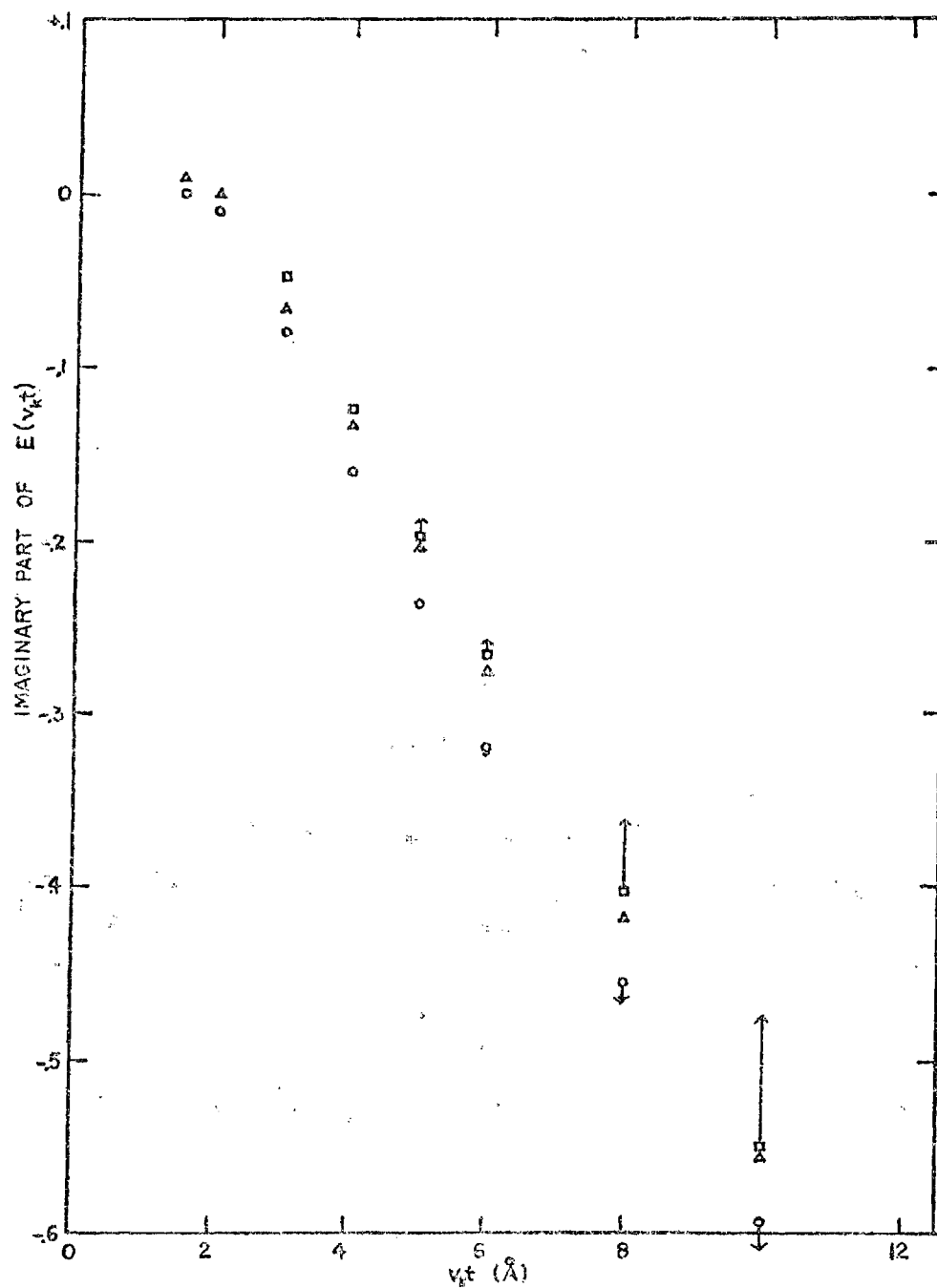
Figure 6. Imaginary Part of $E(v_k t)$. (The circles are evaluated for $k = 14.3 \ \text{Å}^{-1}$ and $r_0 = 2.5 \ \text{Å}$, lower half of error bar shown; triangles, $k = 14.3 \ \text{Å}^{-1}$ and $r_0 = 2.4 \ \text{Å}$; squares, $k = 28.6 \ \text{Å}^{-1}$ and $r_0 = 2.5 \ \text{Å}$, upper half of error bar shown.)

the computed points in Figure 5. The imaginary part of equation (16) is not as smooth and there is noticeable error in its evaluation at large values of $v_k t$. For this reason, no attempt has been made to connect the computed values of the imaginary part by a curve (refer to Figure 6). Where significant, the upper half of the error bar (numerical error only) is shown for $k = 28.6 \text{ Å}^{-1}$, $r_0 = 2.5 \text{ Å}$; and the lower half of the bar for $k = 14.3 \text{ Å}^{-1}$, $r_0 = 2.5 \text{ Å}$. A crude check of E in the region $8 \text{ Å} \leq v_k t \leq 10 \text{ Å}$ indicates that the slope of the real part of E corresponds to a total cross section (according to equation (17)) of $\approx 35 \text{ Å}^2$ for $k = 14.3 \text{ Å}^{-1}$ and $\approx 31 \text{ Å}^2$ for $k = 28.6 \text{ Å}^{-1}$, in rough agreement with the experimentally measured cross section.[23]

Figure 7 contains $R(\vec{k}, v_k \Omega)$ for selected values[22] of k. Plotted in terms of Ω, the width of $R(\vec{k}, v_k \Omega)$ narrows rather slowly as a function of k. From equation (7), it is evident that the width in terms of Ω of the non-condensate contribution evaluated in the impulse approximation is independent of k. The practical implication of this is that if an experiment performed at a given value of k is repeated with a slightly higher value of k, one can only expect a very slight relative sharpening of the condensate portion over the non-condensate. This observation may be somewhat pessimistic since the Lennard-Jones potential used in this calculation is known to be somewhat more repulsive than the actual helium-helium interaction for small distances.[23] However we do not expect that the use of a more realistic potential will change this result significantly.
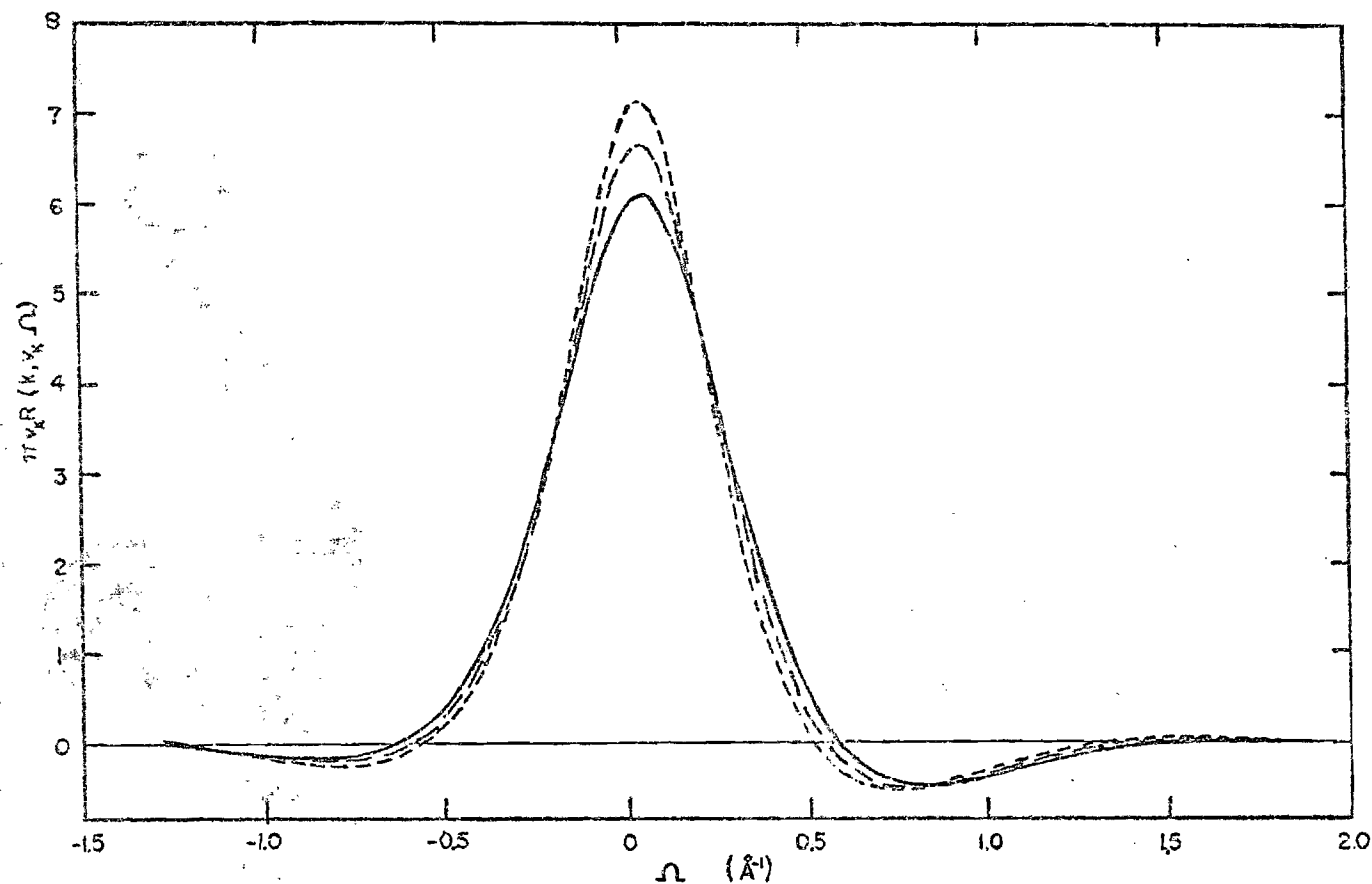
Figure 7. $R(k, v_k \Omega)$ for $r_0 = 2.5$ Å. (The solid line evaluated for $k = 14.3$ Å^{-1}; long-dashed line, $k = 28.6$ Å^{-1}; short-dashed line, $k = 57.2$ Å^{-1}. $\Omega = (\omega - \omega_k)/v_k$.)

On a more optimistic note, the function $R(\vec{k}, v_k\Omega)$ shown in Figure 7 exhibits a non-monotonic behavior as a function of Ω. This characteristic is easily traced back to the short time behavior of the function $E(v_k t)$ defined in equation (15) and exhibited in Figure 5 and 6. This behavior is radically different from the linear in $v_k t$ behavior given by equation (17) for long time. Clearly this occurs because the struck helium particle initially finds itself in an environment of other helium atoms strongly conditioned by the liquid's local structure. The struck helium can travel, on the average, some distance (~ 2 Å to ~ 3 Å) before suffering significant collisions with other helium atoms.

Finally Figure 8 in this section presents the results for the condensate portion of $S(k,\omega)$[22] evaluated for the conditions corresponding to the experiment of Mook, Scherm, and Wilkinson. The condensate part of $S(k,\omega)$ was obtained from $n_o R(k, v_k\Omega)$ assuming that the condensate fraction is 2.4%. Figure 8 also contains the best fitting Gaussian form for the condensate $A_7 \exp[-(\omega - A_8)^2/A_9^2]$ (refer to equation (2) of Chapter II), and that portion of the data judged to be contributed by the condensate. The "condensate" part of the data was obtained by subtracting the first three terms of equation (2) Chapter II from the actual data. It is evident that if $n_o R(k, v_k\Omega)$ were used in place of the "condensate" Gaussian in equation (2) of Chapter II, the best fitting value for the condensate fraction would not be substantially different from the previous estimate[6] of 2.4 $\pm$ 1%. The structure in the energy dependence of the
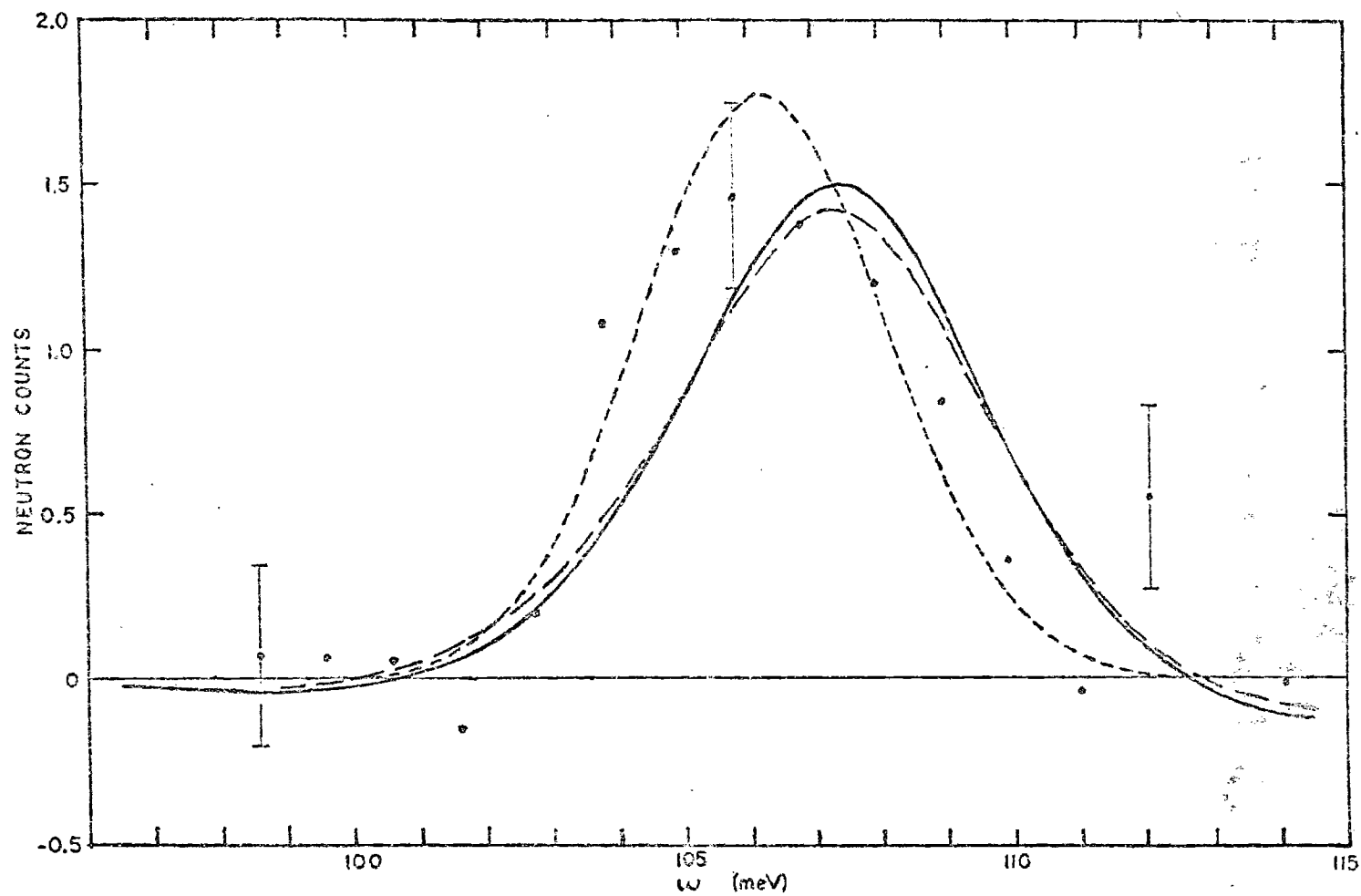
Figure 8. Condensate Contribution to the Dynamic Structure Factor. (The circles are the 'condensate' portion of the data (see text); solid line, theoretical estimate of condensate portion taking $n_o = 2.4\%$ and $r_o = 2.5$ Å; long-dashed line, theoretical estimate taking $n_o = 2.4\%$ and $r_o = 2.4$ Å; short-dashed line, best fit Gaussian with experimental resolution removed.)

experimentally obtained dynamic structure factor is discernible in this figure in the vicinity of 101 meV and 111 meV. The function $n_o R(k, v_k\Omega)$ also has structure which is suggestive of the structure in the data, but the structure in $n_o R$ is located too far from the peak and is less dramatic. The structure in this evaluation of the condensate contribution could be made more pronounced by choosing a significantly larger value for r_o, but then the theta functions $\Theta(|r| - r_o)$ and $\Theta(|\vec{r} + \vec{v}_k t| - r_o)$ (used in equation (13)) would no longer be a reasonable approximation to $g^{1/2}(\vec{r})$ and $g^{1/2}(\vec{r} + \vec{v}_k t)$, respectively. A more precise evaluation of R, in particular the structure in its wings, will probably require a more accurate approximation to $\rho_2(\vec{r}, 0; \vec{r} + \vec{v}_k t, 0)$ than was used in this evaluation.

Extraction of Helium Liquid Properties

Based on the analysis of the experimental data in reference 6 and the results of the analysis in the previous section, one can judge that the condensate contribution to the dynamic structure factor has a full width at half maximum of approximately 5 meV at $k = 14.3 \text{ Å}^{-1}$ while the FWHM of the non-condensate part is roughly 16 meV. In the formulation being used here, the non-condensate part of the dynamic structure factor is given by

$$S_{NC}(k,\omega) = \frac{1}{(2\pi)^2 \rho} \int dp^3 \, n_p \, R(k, v_k\Omega - \vec{v}_k \cdot \vec{p}) \qquad (18)$$

From the above discussion, the FWHM of S_{NC} is approximately 16 meV while the width of R is roughly 5 meV. This suggests that the modified impulse approximation, equation (7), may be used with the recognition that the final-state effects implied by the width of R will be small, though not necessarily negligible. These final-state effects will be considered in the last section of this chapter.

Using the impulse approximation, the extraction of the non-condensate contributions S_{NC} from the experimental data provides an input from which the single-particle momentum distribution, the one-particle density matrix, and the mean kinetic energy per atom in the helium liquid may be calculated. This is discussed in this section.

Taking the partial derivative of the non-condensate part of equation (7) with respect to ω at constant k yields

$$\Omega n_{\Omega} = - (4\pi^2 \rho v_k^2) \frac{\partial S_{NC}}{\partial \omega})_k \qquad (19)$$

The experiment was conducted at a constant scattering angle of $135°$. The momentum transfer, energy transfer, and scattering angle are interrelated by

$$k^2(\theta,\omega) = 2M\{2\epsilon_i [1 - (1 - \omega/\epsilon_i)^{1/2} \cos \theta] - \omega\} \qquad (20)$$

where M is the neutron mass. Using equation (18) and (20), a somewhat uninteresting exercise in partial derivatives leads to

$$\Omega n_{\Omega} = \frac{-4\pi^2 \rho v_{\kappa}^2 \left[\frac{\partial S_{NC}}{\partial \omega}\bigg)_{\theta} + \frac{S_{NC}}{k} \frac{\partial k}{\partial \omega}\bigg)_{\theta} \right]}{\left[1 - v_k\left(1 + \frac{\Omega}{k}\right) \frac{\partial k}{\partial \omega}\bigg)_{\theta} \right]} \qquad (21)$$

where $\Omega = (\omega - \omega_k)/v_k$. As previously noted, the data, as presented in its final form in reference 6 and reporduced here, is proportional to the dynamic structure factor broadened by a resolution function with a FWHM of about 2.1 meV.

For convenience, I chose to use the appropriate portion of the empirical fit (equation (2) of Chapter II), rather than the actual data points, in the application of equation (21). The non-condensate part of the data $I_{NC}(\omega)$ was identified with the non-condensate part of the dynamic structure factor $S_{NC}(\theta,\omega)$ through the relation

$$CI_{NC}(\omega) \cong (\pi\Gamma)^{-1/2} \int_{-\infty}^{\infty} d\varepsilon \ e^{-(\omega-\varepsilon)^2/\Gamma} \ S_{NC}(\theta,\omega) \qquad (22)$$

where

$$I_{NC}(\omega) \equiv A_1 e^{-(\omega-A_2)^2/A_3^2} + A_4 e^{-(\omega-A_5)^4/A_6^4} \qquad (23)$$

$\Gamma = (2.1)^2/(4 \ln2)$ represents the width of the experimental resolution function, and C is a constant to be determined by normalizing the single-particle momentum distribution obtained from equation (21) by means of the relation

$$\sum_{p} n_{p} = 1 \tag{24}$$

The following approximation to the solution of equation (22) was used.

$$S_{NC}(\theta,\omega) \simeq C[A_1{}' \, e^{-(\omega-A_2)^2/A_3'^2} + P(\omega)] \tag{25}$$

where

$$A_1{}' = A_1 A_3 / A_3{}' \tag{26}$$

$$A_3{}' = (A_3{}^2 - \Gamma)^{1/2} \tag{27}$$

$$P(\omega) = A_4 \sum_{n=0}^{4} \frac{1}{n!} (\frac{-\Gamma}{4})^n \, \frac{d^{2n}}{d\omega^{2n}} \, e^{-(\omega-A_5)^4/A_6{}^4} \tag{28}$$

As may be verified by direct substitution, the Gaussian term in equation (25) exactly reproduces the Gaussian in equation (22) after convolution with the resolution function. The polynomial $P(\omega)$ approximately reproduces the term $A_4 \exp[-(\omega-A_5)^4/A_6{}^4]$ of equation (22) after resolution broadening, as verified by numerical integration. The function $P(\omega)$ was obtained from the first five terms of an infinite series solution to an integral equation in the form of equation (22). This series solution is discussed in Appendix F.

The use of equation (25) in equation (21) yields the single-particle momentum distributions shown in Figure 9. Along with the two distributions obtained in this analysis, Figure 9 also contains the distribution found from a Monte Carlo calculation which assumed a Jastrow ground state wave function.[3] To facilitate comparison with the Monte Carlo result, the n_p values determined from the experimental data have been normalized taking the helium density to be 0.022 atoms/$Å^{-3}$ and the condensate fraction to be 0.11 at 1.2°K. Evident from the figure is the large number of atoms carrying a momentum $p \approx 0.7 \, Å^{-1}$ which are not present in the Monte Carlo calculations. The momentum distributions n_p determined from this experiment correspond to the temperatures 1.2°K and 4.2°K, whereas the Monte Carlo calculations were performed for the ground state $T = 0°K$. However, we do not think it likely that the differences in the n_p distributions at $T = 0°K$ and $T = 1.2°K$, shown in Figure 9, are due to this difference in temperature.[15] Some insight into the possible source of this discrepancy is afforded by examination of $\rho_1(0,\vec{r})$, the off-diagonal one-particle density matrix, related to n_p by

$$\rho_1(0, \vec{r}) = \rho \, \Sigma_p n_p e^{i\vec{p}\cdot\vec{r}} \tag{29}$$

For the Monte Carlo calculations, $\rho_1(0,\vec{r})$ is also related to the assumed form of the ground state wave function $\phi(\vec{r}_1, \vec{r}_2, \ldots, \vec{r}_N)$ by
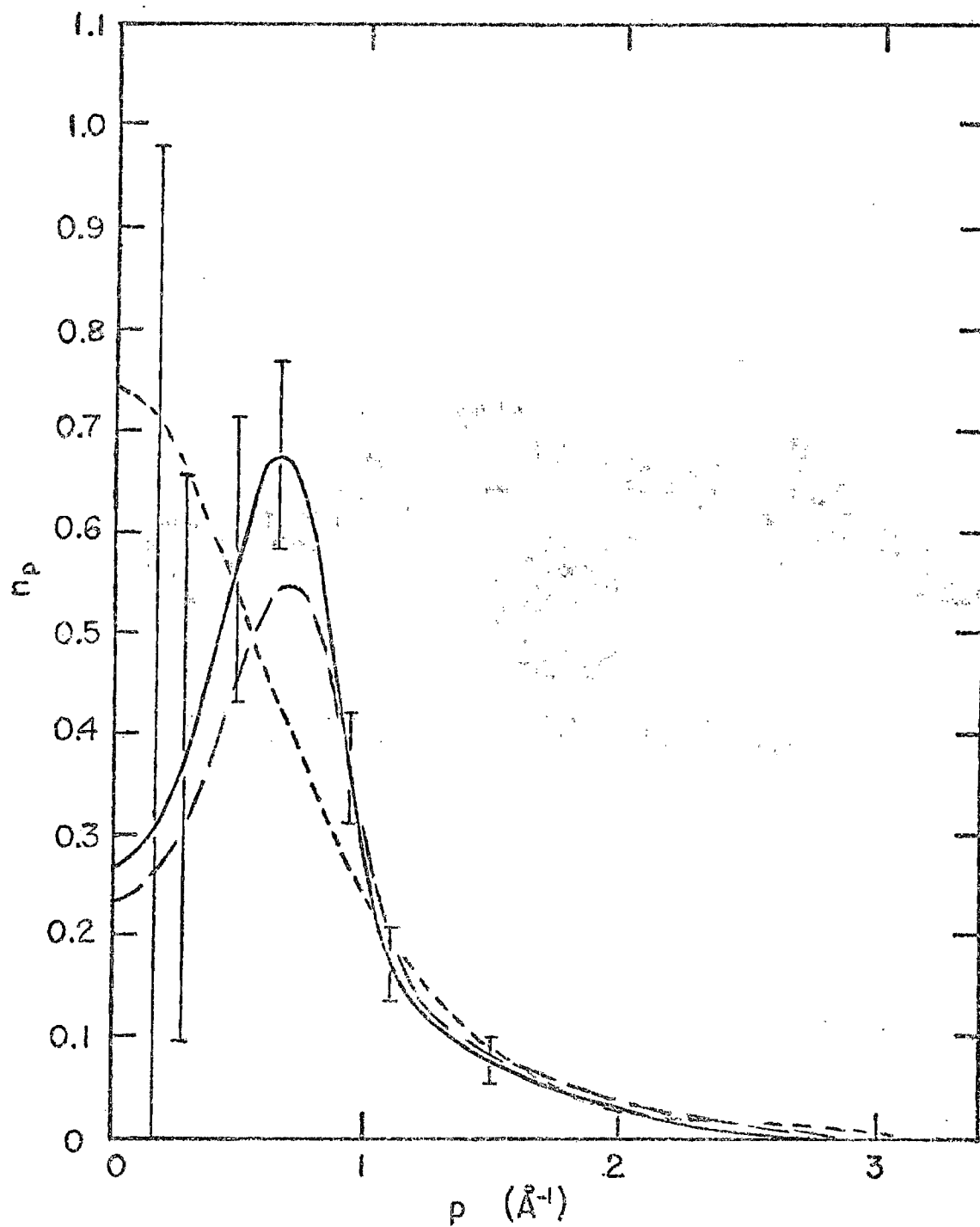
Figure 9. Single-Particle Momentum Distribution via the Impulse
            Approximation. (The solid line is the distribution obtained
            from 1.2°K data; long-dashed line, obtained from 4.2°K data;
            short-dashed line, the result of Monte Carlo calculation
            Ref. 3.)

$$\rho_1(0,r) = \int \phi_0(0, r_2, \ldots, r_N) \quad\quad (30)$$

$$x \quad \phi_0(r, r_2, \ldots, r_N) \, dr_2 \cdots dr_N$$

Figure 10 compares values for $\rho_1(0,r)$ from the experimentally determined n_p values with the Monte Carlo results. The excess atoms carrying momentum ~ 0.7 $\text{\AA}^{-1}$ in Figure 9 give rise to the dip in $\rho_1(0,r)$ near $r \approx 6$ $\text{\AA}$, resulting in a non-monotonic $\rho_1(0,r)$, contrasted with the monotonically decreasing ρ_1 predicted by the computer studies. We believe that the monotonic behavior of $\rho_1(0,r)$ is due to the use, in equation (30) of a Jastrow ground state wave function

$$\psi(r^N) = \prod_{1 \le i \le j \le N} f(r_{ij})$$

for which the assumed form of $f(r)$ is a monotonically increasing function of r, i. e., $f(r) = \exp - (a/r)^5$. Such an $f(r)$ does not account for attractive interactions, which should cause a "bump" in $f(r)$ at an r-value roughly corresponding to the range of the attraction, e. g., $f(r) = \exp[-(a/r)^5 + (b/r)^m]$, $b > 0$, $m > 0$. Graphical estimates of $\rho_1(0,r)$ from equation (30) indicate that the bump in $f(r)$ can produce a non-monotonic $\rho_1(0,r)$. It would be interesting to repeat the Monte Carlo calculations allowing for the effect of attractive interactions between the helium atoms[24] to see
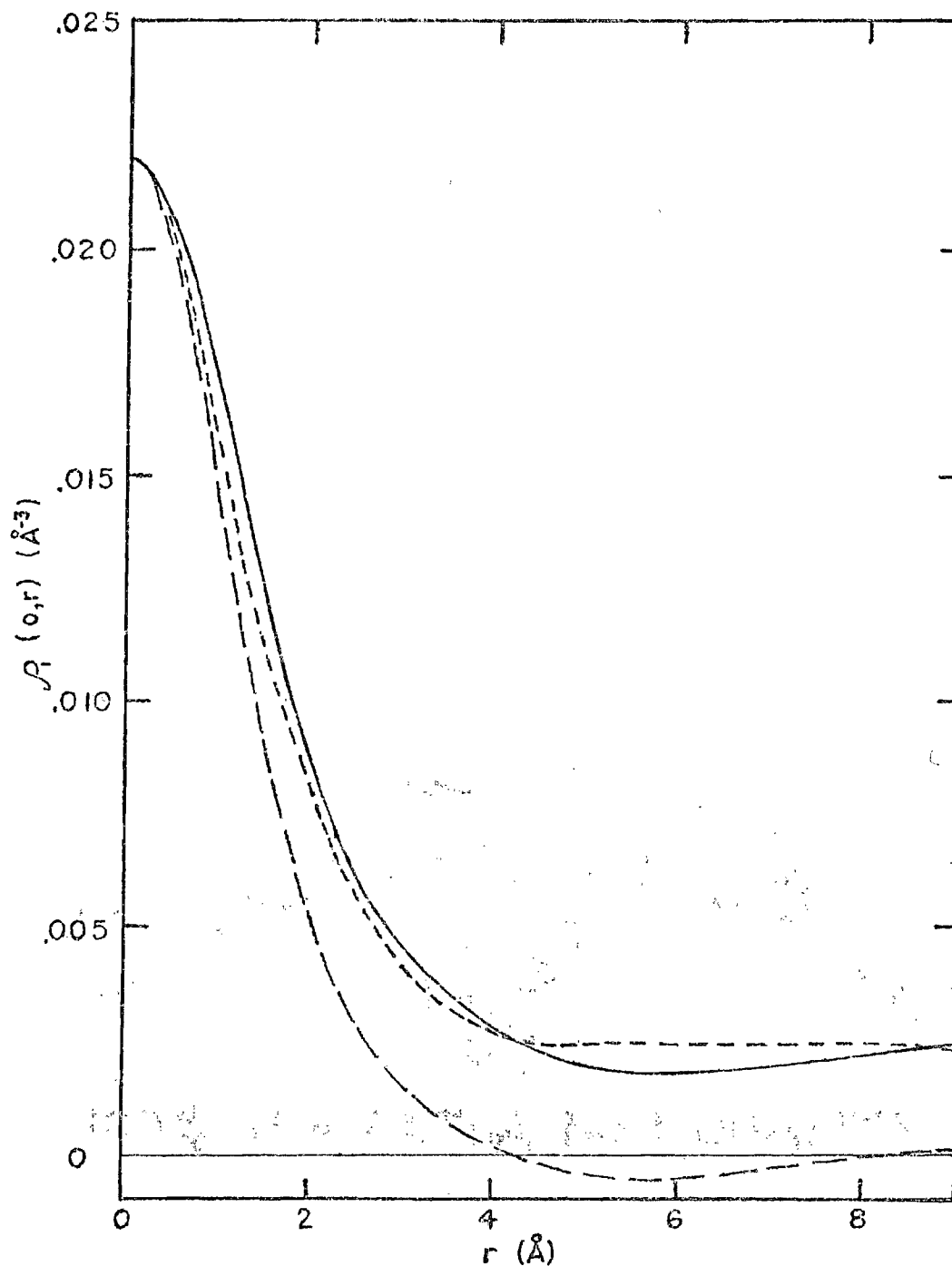
Figure 10. Off-Diagonal One-Particle Density Matrix via Impulse
Approximation. (The solid line is the matrix obtained
from 1.2°K data; long-dashed line, obtained from 4.2°K;
short-dashed line is the result of a Monte Carlo calculation,
Ref. 3.)

if non-monotonic behavior of $\rho(0,r)$ results.

The mean kinetic energy per helium atom is readily obtained from the momentum distribution by calculating the mean-squared momentum. This yields a mean kinetic energy per atom of 12°K/atom at a temperature of 1.2°K and 16°K/atom at 4.2°K. Other estimates for this quantity, obtained from Monte Carlo results for the ground state[3,13] and from experimental data at about 1°K, range from 10.6°K/atom to 15.8°K atom.

Final-State Effects on the Non-Condensate

In the previous section, final-state effects were ignored in obtaining the single-particle momentum distribution and related quantities. This section contains a discussion of the modification of previous results brought about by including the final-state effects embodied in the R function.

The starting point is an expression for the non-condensate contribution to equation (5)

$$S_{NC}(k,\omega) = \frac{1}{4\pi^2\rho} \int_0^\infty p^2 \, dp \, np \int_{-1}^1 \, d\beta R(k, v_k\Omega - v_k p\beta) \tag{31}$$

which has been written in terms of polar coordinates with the change of variable $\beta = \cos\theta$, θ the polar angle. To obtain a formula analogous to equation (19), one takes the partial derivative of equation (31) with respect to ω holding k constant,

$$-4\pi^2 \rho v_k \left.\frac{\partial S}{\partial \omega}\right)_k = \int_0^\infty dp\ pn_p\ R(k,\ v_k\Omega - v_k p) \qquad (32)$$

$$-\int_0^\infty dp\ pn_p\ R(k,\ v_k\Omega + v_k p)$$

The above equation can be written in a slightly more compact form by replacing p by $-p$ in the second integral and artifically extending the definition of n_p to negative values by the prescription $n_{-p} = n_p$. Equation (32) becomes

$$\int_{-\infty}^\infty dp\ pn_p\ R(k,\ v_k\Omega - v_k p) = -4\pi^2 \rho v_k \left.\frac{\partial S}{\partial \omega}\right)_k \qquad (33)$$

The analogous formula for constant scattering angle θ is obtained by taking the partial derivative of equation (31) with respect to ω for constant θ, using equation (20) to interrelate k, ω, and θ. The result is

$$4\pi^2 \rho v_k \left[\left(\frac{\partial S}{\partial \omega}\right)_\theta + \frac{1}{k} S^{NC}\left(\frac{\partial k}{\partial \omega}\right)_\theta\right] = \left[-1 + v_k \left(\frac{\partial k}{\partial \omega}\right)_\theta\right] \qquad (34)$$

$$x \int_{-\infty}^\infty dp\ pn_p\ R(k,\ v_k\Omega - v_k p) + v_k\left(\frac{\partial k}{\partial \omega}\right)_\theta \int_{-\infty}^\infty dp\ \frac{p^2}{k} n_p R(k, v_k\Omega - v_k p)$$

$$+ v_k\left(\frac{\partial k}{\partial \omega}\right)_\theta \int_0^\infty dp\ p^2 n_p \frac{\partial R}{\partial k}$$

where

$$\frac{\partial R}{\partial k} \equiv \frac{\partial}{\partial k} \left. R(k, v_k\Omega - v_k p) \right|_{v_k\Omega - v_k p}.$$

To proceed with determining n_p from the scattering data, one must determine or assume a form for $\partial R/\partial k$. If one wished, $\partial R/\partial k$ could be calculated in a manner similar to the technique used in the second section of this chapter. The expectation that the final-state effects will be small suggests that results of sufficient accuracy could be obtained by just assuming a convenient form for $R(k, v_k\Omega)$, rather than investing in a long, cumbersome evaluation of $\partial R/\partial k$. The author chose to assume a Gaussian form for $R(k, v_k t)$

$$R(k, v_k t) = e^{-(v_k t)^2/\Gamma} \tag{35}$$

which when Fourier transformed yields

$$R(k, v_k\Omega) = \frac{\pi\Gamma}{v_k} e^{-\Omega^2\Gamma/4} \tag{36}$$

This form leads to a considerable simplification of equation (34). From the results of Section II, it is obvious that a Γ may be chosen to yield the correct width and qualitatively the correct shape to mimic the $R(\vec{k}, v_k\Omega - v_k p)$ evaluated in that section. From Figure 7 it can

be seen that the width of $R(\vec{k}, v_k t)$ in terms of $v_k t$ changes by approximately 8 percent as k goes from $k = 14.3 \text{ Å}^{-1}$ to 28.6 Å^{-1}. It therefore appears safe to assume that Γ changes negligibly over the range of k values which are significant for the experimental data being analyzed. Taking Γ as independent of k and inserting equation (36) into equation (34) yields

$$\int_{-\infty}^{\infty} dp \, pn_p \, R(\vec{k}, v_k \Omega - v_k p) \simeq \frac{-4\pi^2 \rho v_k [(\frac{\partial S^{NC}}{\partial \omega})_\theta + \frac{S^{NC}}{k} \frac{\partial k}{\partial \omega})_\theta]}{[1 - v_k \frac{\partial}{\partial \omega})_\theta (1 + \frac{\Omega}{k})]} \quad (37)$$

where approximate equality $\simeq$ is indicated to emphasize that this equation is based on the assumed Gaussian form of $R(\vec{k}, v_k t)$.

The results of Section III may now be reexamined using equation (37). In that section, the right-hand side (RHS) of the above equation was identified as equal to Ωn_Ω (refer to equation (21) and Figure 9) rather than the convolution of R with pn_p. From the general shape of R, one would expect that the convolution of R with pn_p would be broader with less well-defined features than pn_p. This means, for example, that the actual single-particle momentum distribution may have a noticeably sharper peak in the vicinity of $p \simeq .7 \text{ Å}^{-1}$ than indicated in Figure 9.

It is somewhat easier to make a quantitative correction for final-state effects on the previous assessment of the off-diagonal one-particle density matrix. The results for this density matrix,

presented in Section III Figure 10, were obtained from

$$\tilde{\rho}_1(0,r) = \frac{1}{4\pi^2} \int_{-\infty}^{\infty} d\Omega \sin \Omega r \, [\text{RHS of equation (39)}] \qquad (38)$$

In the impulse approximation, the RHS of equation (37) is $\Omega\eta_\Omega$ (refer to equation (21)); and, in this approximation, $\tilde{\rho}$, is quickly shown to be equal to the off-diagonal density matrix $\rho(0,r)$. In the present approximation in which $R(k, v_k t)$ is assumed to be a Gaussian, the RHS of equation (37) is taken as

$$\int_{-\infty}^{\infty} dp \, pn_p \, R(k, v_k\Omega - v_k p),$$

and equation (39) becomes

$$\tilde{\rho}_1(0, r) = \rho_1(0, r)R(k, v_k t = r)$$

where $\tilde{\rho}_1(0,r)$ is the result of the calculation contained in Figure 10 and $\rho_1(0,r)$ is the "true" density matrix. Figure 11 presents the results obtained for $\rho_1(0,r)$ under the assumption that $R(k, v_k t)$ is a Gaussian with $\Gamma = 53.5 \, \text{Å}^2$, the value of Γ being chosen to give a fit to the experimental data comparable to the fit afforded by the condensate (fourth) term of equation (2) of Chapter II.

Figure 11 has been drawn assuming that the condensate fraction n_o is .11. If a significantly smaller value had been chosen for n_o (for example, n_o = .024, a value more consistent with the previous
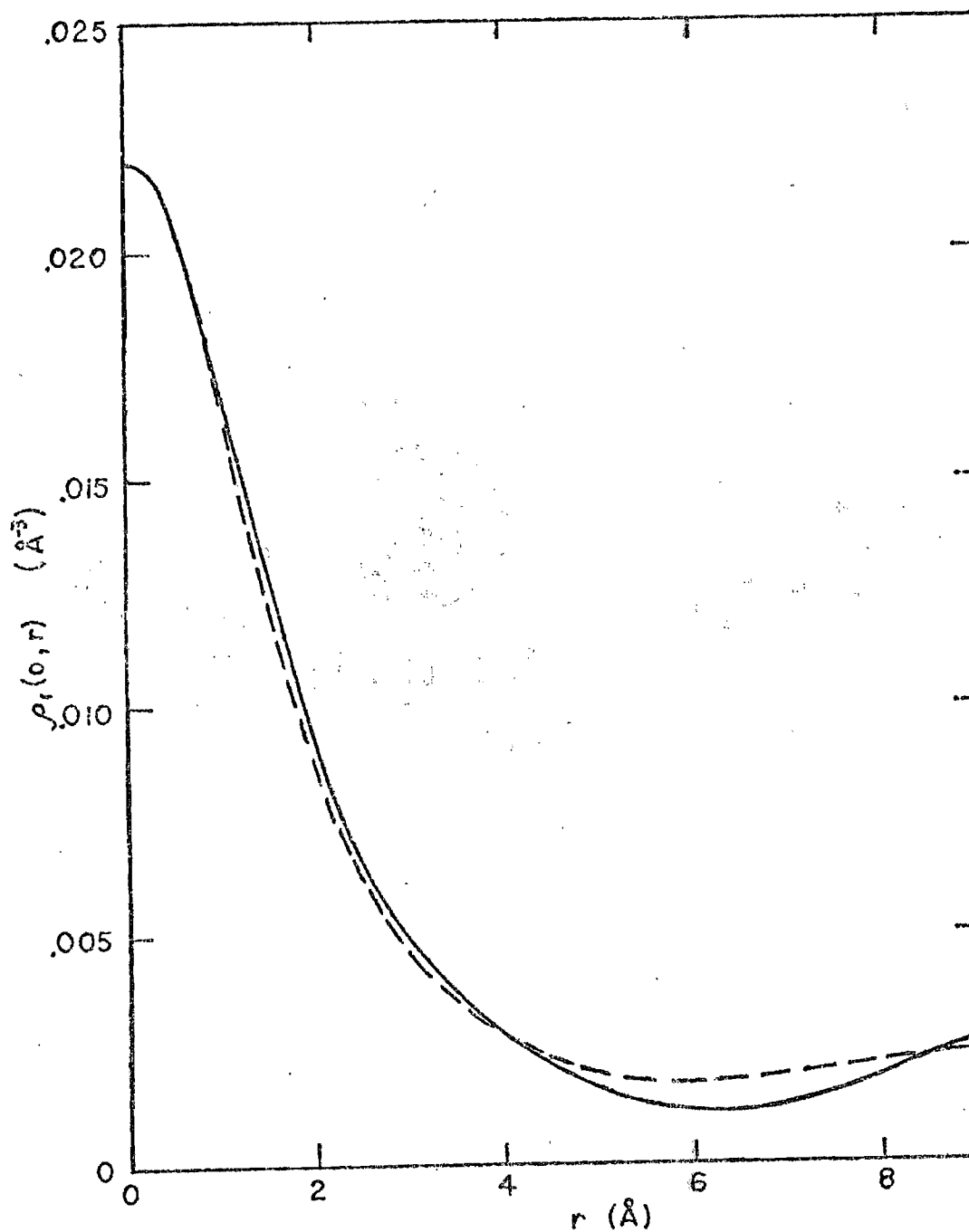
Figure 11. Off-Diagonal One-Particle Density Matrix Corrected for Final-State Effects. (The solid line is the matrix obtained from the 1.2°K data assuming a Gaussian R function (see text); long-dashed line, obtained from 1.2°K data with no correction for final-state effects.)

results), then the resulting $\rho_1(0,r)$ would have negative values for
$r' \approx 6$ Å. This would be incompatible with the assumption that the wave
function of the helium is everywhere non-negative, a zero temperature
assumption utilized in Section II to obtain $R(k, v_k t)$. Since $\rho_1(0,r)$
was evaluated from data taken at a temperature of 1.2°K, the negative
portions of the density might be a real temperature effect, implying
significant deviations of ρ_1 from its ground state shape due to
population of excited states. Another, probably more plausible,
explanation may be that the negative values were artificially
introduced by errors arising from the finite accuracy of the data and
the computational procedure used in the analysis. For example,
theoretical calculations indicate that $n_p \propto 1/p$ for small p. It is
unrealistic to expect an experiment of the type being discussed to
detect this feature. Adding a term to n_p which behaved like 1/p
for small p would diminish the size of the negative values of the
density matrix.

CHAPTER V

CONCLUSIONS

It has been known for many years that the incoherent dynamic
structure factor for a system of non-interacting particles can be
written as a sum of delta-function contributions from each single-
particle momentum state $\vec{p}$ weighted by the fraction of particles $n_{\vec{p}}$
with momentum $\vec{p}$

$$S^{IA}(\vec{k},\omega) = \sum_{\vec{p}} n_{\vec{p}} \; \delta(\omega - k^2/(2m) - \vec{k}\cdot\vec{p}/m) \tag{1}$$

where m is the mass of the non-interacting particles. The formalism
developed here and in Reference 21 shows that the effect of interactions
between the particles is to broaden the delta-function contribution
from the state p into a contribution $R(\vec{k}, \omega - k^2/(2m) - \vec{k}\cdot\vec{p}/m)$ with
non-zero width. Since the evaluation of this function R appears to be
intractable for a realistic many-body system, an approximation to R
has been proposed which takes account of a certain class of final-
state interactions. The final-state interactions included in this
approximation formally resemble multiple single scattering of one of the
particles by its neighbors, evaluated in an eikonal-like approximation.

The R function was evaluated using the Lennard-Jones interaction
and a crude approximation to the two-particle density matrix with the

parameters chosen to resemble superfluid helium. The result was
compared with the assessment of the $p = 0$ contribution to the
dynamic structure factor of superfluid helium obtained from the neutron
scattering data of Mook, Scherm, and Wilkinson. The shape and width of
the theoretically obtained and measured $p = 0$ portion are mutually
supportive. In addition, both exhibit structure in their wings,
although the agreement is only qualitative. The single detrimental
aspect is a significant difference in the location of the peak of
the two functions. No conclusion has been reached on the cause of
this disparity. An auxiliary conclusion based on these results is
that the impulse approximation equation (1) to the dynamic structure
factor of superfluid helium will yield reasonable results for $k \gtrsim 14 \, \overset{\circ}{A}^{-1}$
with only small final-state corrections. The final-state corrections
to the impulse approximation are small for $k = 14.3 \, \overset{\circ}{A}^{-1}$ and decrease
slowly as k increases. This implies that obtaining a significant
improvement in the accuracy of the impulse approximation for the
analysis of neutron scattering data on liquid helium will require the
measurement of the scattering at extremely large momentum transfer,
e. g., $k \approx 50 \, \overset{\circ}{A}^{-1}$. This appears to be beyond the present state of
the art.

The balance of the experimental data was analyzed to obtain
the single-particle momentum distribution, one-particle density matrix,
and the mean kinetic energy per helium atom. The results for the
single-particle momentum distribution indicate a preferential
occupation of the states with momentum $p \approx 0.7 \, \overset{\circ}{A}^{-1}$. This feature is

an entirely new result. The preferential occupation in n_p causes the one-particle density matrix to have damped oscillations in its value at large distances ~ 6 Å. The mean kinetic energy calculated from the data is in reasonable agreement with previous estimates, indicating that the fourth moment of the n_p calculated from the data has an acceptable value.

APPENDIX A

This appendix contains a derivation of the inelastic cross section of neutrons from a target of identical, spinless particles.

Take the initial state of the total system, neutron plus target, to be

$$|i> = L^{-3/2} e^{i\vec{k}_i \cdot \vec{R}} |\phi_i> \qquad (A1)$$

where the neutron is in the box-normalized (volume L^3) plane-wave state $L^{-3/2} \exp(i\vec{k}_i \cdot \vec{R})$ with energy ε_i, and the target is in the initial state $|\phi_i>$ with energy E_i. After the scattering, the system will be in the final state

$$|f> = L^{-3/2} e^{i\vec{k}_f \cdot \vec{R}} |\phi_f> \qquad (A2)$$

the neutron having been scattered into the state with wave-vector $\vec{k}_f$, and the target having undergone a transition to a state $|\phi_f>$ with energy E_f. From first-order, time-dependent perturbation theory, the probability W_{if} of a transition from state i to a state f is

$$W_{if} = \frac{2\pi}{\hbar} \; | \; <i|\tilde{V}|f> |^2 \; \rho_f(\varepsilon_f + E_f) \qquad (A3)$$

Here, $\rho_f(\varepsilon_f + E_f)$ is the density of final states, and $\tilde{V}$ is the interaction which causes the transition. The interaction between a single target particle and the neutron will have a very short range in comparison to the wave-length of a thermal neutron, since the interaction occurs between the neutron and the nucleus of the target particle. It is, therefore, appropriate to represent the neutron-target interaction as a sum of Fermi pseudo-potentials

$$\tilde{V} = \frac{2\pi\hbar^2}{M} \; b \; \sum_j \delta^3(\vec{r}_j - \vec{R}) \qquad (A4)$$

where M is the neutron mass, $\vec{r}_j$ is the position coordinate of the jth target particle, and b is the scattering length which is related to the total cross section σ_b for the scattering of a neutron from a single target particle by

$$\sigma_b = 4\pi \; |b|^2 \qquad (A5)$$

Inserting equation (A3) and (A4) into equation (A2) yields

$$W_{if} = \frac{\sigma_b}{2\hbar} \left(\frac{2\pi\hbar^2}{M}\right)^2 L^{1/6} \tag{A6}$$

$$x \quad \left| \sum_j \langle \phi_f | e^{i(\vec{k}_i - \vec{k}_f)\cdot\vec{r}_j} | \phi_i \rangle \right|^2 \rho_f(\varepsilon_f + E_f) \tag{A6}$$

where the integration of the neutron coordinate R has been performed. The density of final states which conserve energy is

$$\rho_f(\varepsilon_f + E_f) = \left(\frac{L}{2\pi}\right)^3 \frac{Mk_f}{\hbar^2} \, d\Omega' \, d\varepsilon_f \, \delta(\varepsilon_i + E_i - \varepsilon_f - E_f) \tag{A7}$$

where $d\Omega'$ is the differential solid angle.

Noting that the differential cross section is given by W_{if} divided by the incident neutron flux and that the incident flux is the incident neutron velocity $\hbar k_i/M$ times the neutron density $1/L^3$, one finds from the above equations that

$$\frac{d^2\sigma_{if}}{d\Omega' d\varepsilon_f} = \frac{\sigma_b}{4\pi\hbar} \frac{k_f}{k_i} \tag{A8}$$

$$x \quad \left| \sum_j \langle \phi_i | e^{i\vec{k}\cdot\vec{r}_j} | \phi_f \rangle \right|^2 \delta\left(\omega + \frac{E_i}{\hbar} - \frac{E_f}{\hbar}\right)$$

where $\vec{k} = \vec{k}_i - \vec{k}_f$ and $\hbar\omega = \varepsilon_i - \varepsilon_f$.

Most usually, the experimentalists does not attempt to determine the precise initial and final state of the target system. Instead he will measure the total partial differential cross section for all possible scattering processes. This is obtained from equation (A8) by averaging over the initial states and summing over the final states

$$\frac{d^2\sigma}{d\Omega\, d\varepsilon_f} = \frac{\sigma_b}{4\pi\hbar} \frac{k_f}{k_i} \tag{A9}$$

$$x \quad \sum_i P_i \sum_f \left| \sum_j \langle\phi| e^{i\vec{k}\cdot\vec{r}_j} |\phi_f\rangle \right|^2 \delta\left(\omega + \frac{E_i}{\hbar} - \frac{E_f}{\hbar}\right)$$

where P_i is the probability that the system is in state i initially.

Equation (A9) may be made to appear simpler by first representing the delta function as

$$\delta\left(\omega + E_i/\hbar - E_f/\hbar\right) = \frac{1}{2\pi} \int_{-\infty}^{\infty} dt\, e^{-i(\omega + E_i/\hbar - E_f/\hbar)t} \tag{A10}$$

and then using this to rewrite the squared matrix element as

$$\left| \sum_{j} \langle \phi_i | e^{i\vec{k}\cdot\vec{r}_j} | \phi_i \rangle \right|^2 \delta\left(\omega - \frac{E_i}{\hbar} - \frac{E_f}{\hbar}\right) \tag{A11}$$

$$= \frac{1}{2\pi} \int_{-\infty}^{\infty} dt\, e^{-i\omega t} \sum_{j,l} \langle \phi_i | e^{i\vec{k}\cdot\vec{r}_j} | \phi_f \rangle \langle \phi_f | e^{iE_f t/\hbar}\, e^{-i\vec{k}\cdot\vec{r}_j}\, e^{-iE_i t/\hbar} | \phi_i \rangle$$

Noting that

$$\langle \phi_f | e^{iE_f t/\hbar} = \langle \phi_f | e^{iHt/\hbar} \quad \text{and} \quad e^{-iE_i t/\hbar} | \phi_i \rangle = e^{-iHt/\hbar} | \phi_i \rangle$$

where H is the Hamiltonian operator for the target system; equation (A11) may be represented in the form

$$\left| \sum_{j} \langle \phi_i | e^{i\vec{k}\cdot\vec{r}_j} | \phi_f \rangle \right|^2 \delta\left(\omega + E_i/\hbar - E_f/\hbar\right) \tag{A12}$$

$$= \frac{1}{2\pi} \int_{-\infty}^{\infty} dr\, e^{-i\omega t} \sum_{j,l} \langle \phi_i | e^{i\vec{k}\cdot\vec{r}_l} | \phi_f \rangle \langle \phi_f | e^{iHt/\hbar}\, e^{-i\vec{k}\cdot\vec{r}_j}\, e^{-iHt/\hbar} | \phi_i \rangle$$

When equation (A12) is inserted into equation (A9), the sum over final states can be performed trivially by using the completeness relation $\sum_{f} | \phi_f \rangle \langle \phi_f | = 1$, with the result

$$\frac{d^2\sigma}{d\Omega\, d\varepsilon_f} = \frac{\sigma_b}{4\pi\hbar} \frac{k_f}{k_i} \qquad (A13)$$

$$\sum_i P_i \frac{1}{2\pi} \int_{-\infty}^{\infty} d\omega e^{-i\omega t} \sum_{j,l} <\phi_i| e^{i\vec{k}\cdot\vec{r}_l} e^{iHt/\hbar} e^{-i\vec{k}\cdot\vec{r}_j} e^{-iHt/\hbar} |\phi_i>$$

Using standard terminology, the density-density correlation function is defined as $S(\vec{k},t)$

$$S(\vec{k},t) = \sum_j P_i \sum_{j,l} <\phi_i| e^{i\vec{k}\cdot\vec{r}_l} e^{iHt/\hbar} e^{-i\vec{k}\cdot\vec{r}_j} e^{-iHt/\hbar} |\phi_i> \qquad (A14)$$

and its Fourier transform is called the dynamic structure factor $S(\vec{k},\omega)$

$$S(\vec{k},\omega) = \frac{1}{2\pi} \int_{-\infty}^{\infty} dt\, e^{-i\omega t} S(\vec{k},t) \qquad (A15)$$

Comparing equation (A13) and (A15)

$$\frac{d^2\sigma}{d\Omega\, d\varepsilon_f} = \frac{\sigma_b}{4\pi\hbar} \frac{k_f}{k_i} S(\vec{k},\omega) \qquad (A16)$$

This equation appears in Chapter I equation (8).

APPENDIX B

Table 2. The Function $E(v_k t)$.[25]

$k=14.3 \text{ Å}^{-1}$ $r_o=2.4$ Å

$v_k t$ (Å)				$E(v_k t)$			
1.5	.0050633	±	.0001860	+ i(	.010857	±	.000052)
2.0	.0108057	±	.0005052	+ i(	.000102	±	.000201)
3.0	.0894199	±	.0001216	+ i(	-.066365	±	.000105)
4.0	.2827610	±	.0007541	+ i(	-.132535	±	.000368)
5.0	.6124557	±	.00033653	+ i(	-.203699	±	.000632)
6.0	.9984127	±	.010494	+ i(	-.275342	±	.001368)
8.0	1.78945	±	.025166	+ i(	-.417070	±	.000286)
10.0	2.60558	±	.038383	+ i(	-.555588	±	.001589)

$k=14.3 \text{ Å}^{-1}$ $r_o=2.5$ Å

$v_k t$ (Å)				$E(v_k t)$			
1.5	.0032151	±	.000402	+ i(	.000816	±	.000050)
2.0	.00560	±	.00031	+ i(	-.010169	±	.000094)
3.0	.04485			+ i(	-.079724		)
4.0	.203638	±	.000022	+ i(	-.160225	±	.000352)
5.0	.49991	±	.000239	+ i(	-.2367	±	.0021)
6.0	.88640	±	.00474	+ i(	-.32062	±	.00284)
8.0	1.66917	±	.00269	+ i(	-.455	±	.01)
10.0	2.47756	±	.00506	+ i(	-.593	±	.015)

$k=28.6 \text{ Å}^{-1}$ $r_o=2.5$ Å

$v_k t$ (Å)				$E(v_k t)$			
2.0	.0026167	±	.000395	+ i(	-.005005	±	.000104)
3.0	.0152570			+ i(	-.047793		)
4.0	.1368068	±	.0005317	+ i(	-.123967	±	.00018)
5.0	.39161	±	.004349	+ i(	-.197043	±	.01108)
6.0	.728346	±	.014289	+ i(	-.266276	±	.00548)
8.0	1.404331	±	.007141	+ i(	-.409753	±	.04917)
10.0	2.084995	±	.116426	+ i(	-.549866	±	.07544)

Table 2. (Continued).

$v_k t$ (Å)	k=42.9 Å^{-1}			E($v_k t$)	r_0=2.5 Å	
2.0	.0016898	±	.0001263	+ i(- .0024584	±	.0000333)
3.0	.0053789	±	.0005033	+ i(- .0250815	±	.0001325)
4.0	.8991887	±	.0004701	+ i(- .0951216	±	.0000732)
5.0	.3158323	±	.0009093	+ i(- .1636986	±	.0009487)
6.0	.6193929	±	.0019012	+ i(- .2324432	±	.001864)
8.0	1.2272486	±	.0034674	+ i(- .3684462	±	.003102)
10.0	1.836066	±	.0041142	+ i(- .504009	±	.004373)

$v_k t$ (Å)	k=57.2 Å^{-1}			E($v_k t$)	r_0=2.5 Å	
2.0	.0019992	±	.0001375	+ i(- .0032993	±	.0000169)
3.0	.0080329	±	.0002937	+ i(- .0331044	±	.0000147)
4.0	.1075794	±	.0004451	+ i(- .1064559	±	.0003307)
5.0	.3479725	±	.0007225	+ i(- .1733519	±	.0012142)
6.0	.6689186	±	.0034939	+ i(- .2355611	±	.0062597)
8.0	1.3132175	±	.0080384	+ i(- .3589165	±	.0172025)
10.0	1.9600907	±	.0115676	+ i(- .4818579	±	.0283641)

Table 3. The Function $R(k,v,\Omega)$ Evaluated at Constant k.[25,26] (The values of $v_k R(k,v_k\Omega)$ are tabulated in Å units; $r_o = 2.5$ Å.)

Ω (Å^{-1})	$\pi v_k R(k,v_k\Omega)$ kΩ^{-1} $k=14.3$ Å^{-1}	$\pi v_k R(k,v_k\Omega)$ kΩ^{-1} $k=28.6$ Å^{-1}	$\pi v_k R(k,v_k\Omega)$ kΩ^{-1} $k=42.9$ Å^{-1}	$\pi v_k R(k,v_k\Omega)$ kΩ^{-1} $k=57.2$ Å^{-1}
-1.20	- .02863	- .03154	- .02607	- .02425
-1.10	- .07119	- .07932	- .07415	- .07277
-1.00	- .11718	- .13414	- .13168	- .13062
- .90	- .15422	- .18275	- .18660	- .18580
- .80	- .16123	- .20297	- .21750	- .21725
- .70	- .10482	- .16099	- .19027	- .19186
- .65	- .03793	- .10206	- .13968	- .14323
- .60	.06511	- .00772	- .05374	- .06031
- .55	.21373	.13134	.07757	.06660
- .50	.41854	.32596	.26609	.24905
- .45	.69100	.58855	.52563	.50074
- .40	1.04264	.93279	.87176	.83745
- .35	1.48356	1.37287	1.32115	1.27691
- .30	2.01995	1.92151	1.88958	1.83698
- .25	2.65011	2.58623	2.58778	2.53241
- .20	3.35895	3.36245	3.41342	3.36717
- .15	4.11156	4.22302	5.84116	4.32077
- .10	4.84820	5.10521	5.29109	5.32818
- .05	5.48512	5.90197	6.14680	6.26055
.00	5.92669	6.47081	6.73750	6.92914
.05	6.09022	6.67366	6.90612	7.14144
.10	5.93542	6.43878	6.58514	6.80241
.15	5.48198	5.80370	5.84116	5.98326
.20	4.80304	4.89968	4.84052	4.88337
.25	3.99853	3.88973	3.76692	3.72152
.30	3.16503	2.90935	2.75789	2.65354
.35	2.37624	2.04151	1.88771	1.75520
.40	1.67742	1.32129	1.18062	1.04378
.45	1.08917	.75192	.63135	.50536
.50	.61475	.31989	.22106	.11396
.55	.24696	.00542	- .07314	- .15825
.60	- .02661	- .21355	- .27352	- .33661
.65	- .22027	- .35559	- .39982	- .44260
.70	- .34826	- .43797	- .46883	- .49383
.80	- .42371	- .47818	- .48799	- .48604
.90	- .44306	- .41988	- .41422	- .39604
1.00	- .36427	- .31867	- .30178	- .27600
1.10	- .26284	- .20889	- .18468	- .15756
1.20	- .16405	- .11022	- .08259	- .05830
1.30	- .08174	- .03232	- .00504	- .01410

Table 4. Condensate Contribution to $S(k,\omega)$ for the Experimental Conditions of Mook, Scherm, and Wilkinson. (Condensate fraction taken to be 2.4%; values of $n R(k,\omega)$, the condensate contribution, expressed in neutron counts per 20 minute counting interval.)

Energy ω (meV)	$n_o R(k,\omega)$ $r_o=2.5\text{Å}$	$n_o R(k,\omega)$ $r_o=2.4\text{ Å}$
97	- .03009	- .02811
98	- .03811	- .03026
99	- .03842	- .02287
100	- .02229	.00175
101	.02107	.05477
102	.11091	.15148
103	.26896	.31046
104	.51656	.54819
105	.85538	.86194
106	1.22720	1.19482
107	1.47954	1.40950
108	1.44340	1.36137
109	1.12254	1.06138
110	.69914	.67377
111	.33676	.49611
112	.09206	.11727
113	- .04519	.04195
114	- .10503	- .07409

Table 5. Non-Condensate Single-Particle Momentum Distribution[27] Evaluated via the Impulse Approximation.

Momentum p (Å^{-1})	n_p at 1.2°K	Momentum p (Å^{-1})	n_p at 4.2°K
.083397	.278358	.083143	.242654
.166786	.306380	.166279	.262231
.250171	.353758	.249415	.295230
.333560	.419877	.332557	.341309
.416959	.500384	.415711	.398038
.500374	.584115	.498884	.459139
.583811	.651208	.582081	.513141
.667277	.675728	.665309	.544045
.750778	.636154	.748574	.535881
.834321	.531804	.831883	.481357
.917911	.392675	.915242	.390269
.931970	.367372	.929063	.371317
1.01989	.244654	1.01603	.268552
1.10783	.171489	1.10303	.191325
1.19580	.134703	1.19007	.146443
1.28380	.112884	1.27715	.122298
1.37185	.096017	1.36429	.106441
1.45995	.081594	1.45148	.093380
1.54811	.068948	1.53874	.081733
1.63633	.057800	1.62607	.071164
1.72463	.048015	1.71349	.061550
1.81301	.039510	1.80100	.052846
1.81254	.039555	1.81900	.050980
1.90469	.031938	1.91112	.042955
1.99690	.025530	2.00330	.035897
2.08918	.020208	2.09555	.029756
2.18155	.015841	2.18788	.024470
2.27400	.012302	2.28030	.019965
2.36656	.009466	2.37283	.016165
2.45922	.007219	2.46546	.012990
2.55200	.005458	2.55822	.010362
2.64492	.004092	2.65110	.008206
2.73797	.003042	2.74413	.006453
2.76916	.002801	2.77486	.005981
2.86659	.002050	2.87662	.004582
2.96413	.001491	2.97846	.003493
3.06181	.001078	3.08038	.002651
3.15964	.000775	3.18241	.002004
3.25762	.000554	3.28455	.001510
3.35577	.000394	3.38682	.001133
3.45410	.000278	3.48924	.000848
3.55262	.000196	3.59180	.000632

Table 6. One-Particle Density Matrix[25,27] Evaluated via Impulse
          Approximation.

r (Å)	$\rho_1(0,r)$ at 1.2°K (Å⁻³)	$\rho_1(0,r)$ at 4.2°K (Å⁻³)
0.001	.0219970	.0219832
0.501	.0204721	.0197575
1.001	.0167036	.0145508
1.501	.01236147	.00915143
2.001	.00873689	.00524222
2.501	.00621908	.00290662
3.001	.00459965	.00156527
3.501	.00354098	.000721777
4.001	.002812129	.000140819
4.501	.002307337	-.000249961
5.001	.001986381	-.000474902
5.501	.001825687	-.000555237
6.001	.001796807	-.000524000
6.501	.001863837	-.000422404
7.001	.001988661	-.000287937
7.501	.002135939	-.000152540
8.001	.002277142	-.0000393385
8.501	.0023929738	.0000400297
9.001	.0024735940	.0000832362
9.501	.0025175094	.0000950127
10.001	.002529422	.0000838470
10.501	.0025178208	.0000599873
11.001	.0024925318	.0000329291
11.501	.0024625590	.00000889558
12.001	.0024349499	-.00000817188

Table. 7. Experimental Data[6,28].

Energy (meV)	S(k,ω) at 1.2°K (Neutron Counts per 20-Min. run)	S(k,ω) at 4.2°K (Neutron Counts per 20-Min. run)	Experimental Error)± Counts)
72.73	12.8	13.1	.8
79.00	13.4	13.6	.8
85.16		14.7	.8
89.30	15.3	15.0	.8
93.41	17.8	18.4	.52
95.51	19.1	20.3	.52
97.56	21.6	22.4	.52
98.59	24.4	24.2	.28
99.60	26.7	26.0	.28
100.62	28.8	27.3	.28
101.61	30.2	28.5	.28
102.72	31.8	29.7	.28
103.80	33.4	30.4	.28
104.88	34.0		.28
105.78	34.3	31.0	.28
106.81	34.2		.28
107.94	33.8	30.5	.28
108.94	33.0	30.0	.28
109.90	31.8	29.3	.28
110.98	30.1	28.5	.28
112.03	28.9	27.3	.28
113.07	26.3	25.6	.28
114.08	23.8	24.2	.52
116.16	20.1	21.0	.52
118.24	17.5	18.2	.52
122.37	14.8	15.7	.8
128.53	13.4	14.1	.8
134.76	12.9	13.3	.8

APPENDIX C

In this Appendix, an outline of the derivation of the following

identity is given

$$Te^{\displaystyle iH(t - t_o) + i \int_{t_o}^{t} \frac{U_j(v_k t')dt'}{U_j(v_k t')dt'}} \tag{C1}$$

$$= Te^{\displaystyle i \int_{t_o}^{t} e^{iH(t-t')} U_j(v_k t')e^{-iH(t-t')} \, dt'} e^{iH(t-t_o)}$$

which, for $t_o = 0$ is equation (11) of Chapter III. The validity of

this identity will be shown by a direct iterative method. More

sophisticated proofs of this identity are possible (for example, by

differentiating both sides of (C1) with respect to t_o and rearranging).

Begin by defining the left side of (C1) as $U(t-t_o)$:

$$U(t-t_o) = Te^{\displaystyle iH(t-t_o) + i \int_{t_o}^{t} U_j(v_k t')dt'} \tag{C2}$$

One wishes to show that $U(t-t_o)$ can be rewritten as the right side of

equation (C1). The time derivative of U is

$$\frac{dU(t-t_o)}{dt} = i[H + U_j(v_k t)]U(t-t_o) \qquad (C3)$$

The equivalent integral equation for U is

$$U(t-t_o) = e^{iH(t-t_o)} + i\int_{t_o}^{t} e^{iH(t-t')} U_j(v_k t')U(t'-t_o)dt' \qquad (C4)$$

The iterated solution to equation (C4) is

$$U(t-t_o) = e^{iH(t-t_o)} + i\int_{t_o}^{t} e^{iH(t-t')} U_j(v_k t')e^{iH(t'-t_o)}dt' \qquad (C5)$$

$$+i^2\int_{t_o}^{t} e^{iH(t-t')} U_j(v_k t')dt'\int_{t_o}^{t'} e^{iH(t'-t'')} U_j(v_k t'')e^{iH(t''-t_o)}dt'' +...$$

By manipulating the times appearing in the exponentials, one can factor out the operator exp $[iH(t-t_o)]$:

$$U(t-t_o) = \left\{ 1 + i \int_{t_o}^{t} e^{iH(t-t')} U_j(v_k t') e^{-iH(t-t')} dt' \right. \qquad (C6)$$

$$+ i^2 \int_{t_o}^{t} e^{iH(t-t')} U_j(v_k t') e^{-iH(t-t')} dt' \int_{t_o}^{t'} dt'' e^{iH(t-t'')} U_j(v_k t'') \left. \right\}$$

$$e^{-iH(t-t'')} + \ldots e^{iH(t-t_o)}$$

The factorization of $\exp[iH(t-t_o)]$ is possible in all higher orders, and the terms in curly brackets (C6) produce the time-ordered operator on the right side of (C1):

$$U(t-t_o) = Te^{i \int_{t_o}^{t} e^{iH(t-t')} U_j(v_k t') e^{-iH(t-t')} dt'} e^{iH(t-t_o)} \qquad (C7)$$

which completes the demonstration.

APPENDIX D

In this appendix an expansion is developed for a time-ordered operator which resembles the cumulant expansion of an exponential operator. The expansion will be applied to $S(\vec{k},t)$,

$$NS(\vec{k},\ t) = e^{i\omega_k t}\ \sum_{j,l}\ \Big\langle e^{-i\vec{k}\cdot(\vec{r}_j - \vec{r}_l)}$$

$$e^{i\vec{p}_j \cdot \vec{v}_k t}\ Te^{i\int_{t_o}^t e^{iH(t-t')} U_j(v_k t') e^{-iH(t-t')} dt'}\Big\rangle \tag{D1}$$

which may be rewritten as

$$S(\vec{k},\ t) = e^{i\omega_k t}\ \Big\langle \Big\{ \sum_l e^{-i\vec{k}\cdot(\vec{r}_l - \vec{r}_l)} e^{i\vec{p}_l \cdot \vec{v}_k t} e^{iHt} \Big\} \tag{D2}$$

$$X\ Te^{i\int_{t_o}^t dt' e^{-iHt'} \sum_{m\neq l}[V(\vec{r}_l - \vec{v}_k t',\ \vec{r}_m) - V(\vec{r}_l,\ \vec{r}_m)]e^{+iHt'}} \Big\{ e^{iHt} \Big\} \Big\rangle$$

The technique will be to find $E(t)$, such that

$$e^{-E(t)} = \left\langle \theta_1 \left\{ Te^{i \int_{t_o}^{t} dt' \sum_m \theta_m (t')} \right\} \theta_2 \right\rangle \tag{D3}$$

where θ_1, $\sum_m \theta_m (t')$, and θ_2 are arbitrary operators later to be chosen so that equation (D3) can be applied to equation (D2).

Taking the logarithm of equation (D3) yields

$$E(t) = -\ln \left\langle \theta_1 Te^{i \int_{t_o}^{t} dt' \sum_m \theta_m(t')} \theta_2 \right\rangle \tag{D4}$$

Introduce a parameter λ and two operators $\Gamma_m(t)$ and $\theta_m(t,\lambda)$, such that

$$1 - \Gamma_m = Te^{i \int_{t_o}^{t} dt' \theta_m(t')} \tag{D5}$$

$$1 - \lambda\Gamma_m = Te^{i \int_{t_o}^{t} dt' \theta_m(t',\lambda)} \tag{D6}$$

Note from equations (D5) and (D6) that the partial time derivative of equation (D6) is

$$\lambda\theta_m(t)Te^{i\int_{t_o}^{t} dt' \theta(t')} = \theta_m(t,\lambda)Te^{i\int_{t_o}^{t} dt' \theta_m(t',\lambda)} \qquad (D7)$$

From the above three equations, the following properties of $\theta_m(t,\lambda)$ may be deduced:

$$\theta_m(t, 0) = 0, \qquad (D8)$$

$$\theta_m(t, 1) = \theta_m(t), \qquad (D9)$$

$$\frac{\partial \theta_m(t,\lambda)}{\partial \lambda}\Bigg]_{\lambda=0} = \theta_m(t)Te^{i\int_{t_o}^{t} dt' \theta_m(t')} \qquad (D10)$$

$$\frac{\partial^2 \theta_m(t,\lambda)}{\partial \lambda^2}\Bigg]_{\lambda=0} = 2\theta_m(t)Te^{i\int_{t_o}^{t} dt' \theta_m(t')}\left(1-Te^{i\int_{t_o}^{t} dt' \theta_m(t')}\right) \qquad (D11)$$

etc.

Defining

$$E(t,\lambda) = -\ln\left\langle \theta_1 Te^{i\int_{t_o}^{t} dt' \sum_m \theta_m(t'm\lambda)} \theta_2 \right\rangle \qquad (D12)$$

one can see from equation (D9) that $E(t) = E(t,1)$ and from equation (D8) and (D12) that $E(t,0) = -\ln \theta_1 \theta_2$. Assume $E(t,\lambda)$ is analytic in λ in the closed unit circle. $E(t)$ may then be obtained by expanding $E(t,\lambda)$ in a Taylor's series about $\lambda = 0$, evaluated at $\lambda = 1$.

$$E(t) = E(t,0) + \frac{\partial E(t,\lambda)}{\partial \lambda}\bigg]_{\lambda=0} + \frac{1}{2!} \frac{\partial^2 E(t,\lambda)}{\partial \lambda^2}\bigg]_{\lambda=0} + \ldots \quad (D13)$$

With the use of equations (D10) through (D12), the partial derivatives of $E(t,\lambda)$ with respect to λ, evaluated at $\lambda = 0$, may be obtained. This allows one to rewrite equation (D13) as

$$-E(t) = \ln\langle\theta_1\theta_2\rangle - \sum_m \frac{\langle\theta_1 \Gamma_m(t) \theta_2\rangle}{\theta_1\theta_2} \quad (D14)$$

$$+ \left\{ \sum_{m_1 \neq m_2} \frac{\left\langle\theta_1 \int_{t_o}^{t} dt_1 \int_{t_o}^{t} dt_2 \frac{\partial \Gamma_{m_1}(t_1)}{\partial t_1} \frac{\partial \Gamma_{m_2}(t_2)}{\partial t_2} \theta_2\right\rangle}{\langle\theta_1\theta_2\rangle} \right.$$

$$\left. - \frac{\left\langle\theta_1 \sum_m \Gamma_m(t)\theta_2\right\rangle^2}{2\langle\theta_1\theta_2\rangle^2} \right\} + \ldots$$

where the first three terms of the Taylor's series, equation (D13),
are shown explicitly. The final result is

$$\theta_1 \left[Te^{i\int_{t_o}^{t} dt' \sum_m \theta_m(t')} \right] \theta_2 = \langle \theta_1 \theta_2 \rangle \exp[\omega_1 + \omega_2 + \ldots] \quad (D15)$$

$$\omega_1 = -\sum \langle \theta_1 \Gamma_m(t) \theta_2 \rangle / \langle \theta_1 \theta_2 \rangle$$

$$\omega_2 = \sum_{m_1 \neq m_2} \langle \theta_1 \int_{t_o}^{t} dt \int_{t_o}^{t} dt_2 \frac{\partial \Gamma_{m_1}(t_1)}{\partial t_1} \frac{\partial \Gamma_{m_2}(t_2)}{\partial t_2} \theta_2 \rangle / \langle \theta_1 \theta_2 \rangle$$

$$- \frac{1}{2} \langle \theta_1 \sum_m \Gamma_m(t) \theta_2 \rangle^2 / \langle \theta_1 \theta_2 \rangle \quad (D16)$$

Identifying the θ_j operators to apply these results to (D2) yields the
value for ω_1 quoted in equation (18) of Chapter III.

APPENDIX E

This appendix contains a demonstration that the function

$$E(v_k t) = \rho \int dr^3 \theta(|\vec{r}| - r_0)\theta(|\vec{r} + v_k t| - r_0)$$ (E1)

$$\left[1 - e^{\frac{i}{v_k} \int_0^{v_k t} dy[V(\vec{r} + \vec{y}) - V(\vec{r} + \vec{v}_k t)]} \right]$$

which is defined in Chapter IV equation (16), is dominated by a term

linear in $v_k t$ for sufficiently large values of $v_k t$. This result will

be obtained by assuming that maximum range R_m beyond which the potential

is essentially zero, i. e.,

$$V(r) \approx 0 \text{ for } r \gtrsim R_m$$ (E2)

Examining equation (E1), note that the phase factor in the

imaginary exponential is obtained by integrating the potential along the

line segment which connects the "initial" position $\vec{r}$ to the final

position $\vec{r} + \vec{v}_k t$. If the initial position $\vec{r}$ is such that the potential

is zero along this whole line segment, then the phase factor vanishes

and this particular "configuration" makes no contribution to the value of

$E(v_k t)$. Only those configurations for which part or all of the associated

line segment passes within a distance R_m of the origin will contribute

to $E(v_k t)$. One may decompose the configurations which do contribute

into the three disjoint classes illustrated in Figure 12.

Consider E_{sr} and E_{sp}; the "start" and "stop" contributions to

$E(v_k t)$, respectively. The evaluation of each of these two requires

the integration of a bounded function over a finite volume; therefore,

both E_{sr} and E_{sp} are bounded. A bound is

$$|\text{Real Part } E_{sr}|, \quad |\text{Real Part } E_{sp}| \leq 2\pi\rho R_m^3/3 \quad \text{(E3)}$$

$$|\text{Imaginary Part } E_{sr}|, \quad |\text{Imaginary Part } E_{sp}| \leq 2\pi\rho R_m^3/3 \quad \text{(E4)}$$

Now considering the "through" contributions, rewrite this part

in cylindrical coordinates (b,z,θ)

$$E_t(v_k t) = 2\pi\rho \int_0^\infty b \, db \int_{-\infty}^\infty dz \, \theta(|\vec{r}| - r_0)\theta(|\vec{r} + v_k t| - r_0) \quad \text{(E5)}$$

$$x \left[1 - e^{\frac{i}{v_k} \int_0^{v_k t} dy[V(b,z+y) - V(b, z + v_k t)]} \right]$$

where the integration is restricted to a volume V_T corresponding to

through scattering (it is assumed that the potential is cylindrically

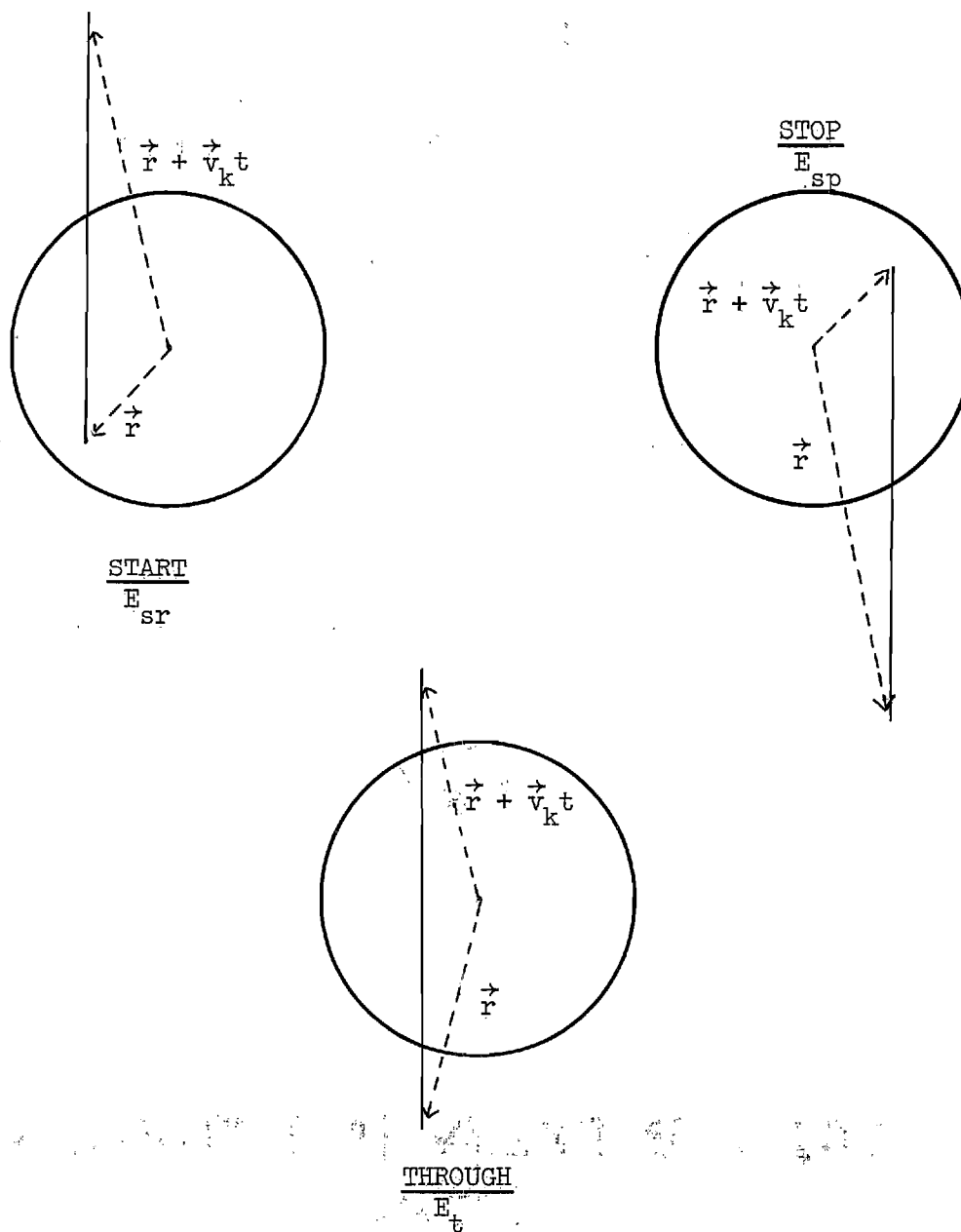symmetric about the z-direction). The theta functions are identically

Figure 12. Contributions to $E(v_k t)$. (Drawn for $v_k t > 2R_m$ (see test). Circles of radius R_m, indicating maximum range of $V(r)$.)

unity for through scattering and so may be dropped. The upper limit on the db-integration may be replaced by R_m, since the potential is zero outside that distance (refer to equation (E2)). By studying Figure 12, one may determine the appropriate limits on the dz-integration for the through contribution. For $v_k t \geq 2R_m$, the result is

$$E_t(v_k t) = 2\pi\rho \qquad (E6)$$

$$x \int_0^{R_m} b\,db \int_{z^-}^{z^+} dz \left[1 - e^{\frac{i}{v_k} \int_0^{v_k t} dy\, [V(b,z+y) - V(b,z+v_k t)]} \right]$$

where $z^+ = -(R_m^2 - b^2)^{1/2}$ and $z^- = z^+ - v_k t$. This equation may be simplified by noting that $V(\vec{r} + \vec{v}_k t)$ is zero and that the limits on the dy-integration may be extended to $\pm \infty$, since for through scattering the parts of the line segment $\vec{r} + \vec{y}$ for $y \geq v_k t$ and for $y \leq 0$ pass through regions where the potential is zero. Applying these observations and making the change of variables $z' = z + y$ yields

$$E_t(v_k t) = 2\pi\rho \qquad (E7)$$

$$x \int_0^{R_m} b\,db \int_{z^-}^{z^+} dz' \left[1 - e^{\frac{i}{v_k} \int_{-\infty}^{\infty} dz' V(b,z')} \right]$$

Performing the dz-integration produces

$$E_t(v_k t) = 2\pi\rho \tag{E8}$$

$$x \int_0^{R_m} b\,db \left[1 - e^{\frac{i}{v_k} \int_{-\infty}^{\infty} dz' V(b,z')} \right] \left[v_k t - 2(R_m^2 - b^2)^{1/2} \right]$$

The total $E(v_k t)$ is now given by

$$E(v_k t) = v_k t \, 2\pi\rho \int_0^{R_m} b\,db \left[1 - e^{\frac{i}{v_k} \int_{-\infty}^{\infty} dz \, V(b,z)} \right] \tag{E9}$$

$$- 2\pi\rho \int_0^{R_m} b\,db \, \{2(R_m^2 - b^2)^{1/2}\}\{1 - e^{\frac{i}{v_k} \int_{-\infty}^{\infty} dz \, V(b,z)} \}$$

$$+ E_{sr} + E_{sp}$$

As observed previously, E_{sr} and E_{sp} are bounded (refer to equation (E3) and (E4). In addition, the second term in equation (E9) is bounded. Therefore, the above equation may be written as

$$E(v_k t) = v_k t \, 2\pi\rho \int_0^{R_m} b\,db \, 1 - e^{(i/v_k) \int_{-\infty}^{\infty} dz \, V(b,z)} + C \tag{E10}$$

where C is bounded for all values of $v_k t$. Converting the polar integration bdb into an integration over the cartesian coordinates dxdy

(after having extended the limit on the bdb integration from R_m to $\pm \infty$), equation (E10) becomes

$$E(v_k t) = v_k t \rho \int_{-\infty}^{\infty} \int_{-\infty}^{\infty} dxdy \left[1 - e^{\frac{i}{v_k} \int_{-\infty}^{\infty} dz V(x,y,z)} \right] + C \qquad (E11)$$

The integral shown explicitly in equation (E11) is simply related to the forward scattering amplitude $f_e(k,k)$ evaluated in the eikonal approximation[29]

$$f_e(k,k) = \frac{ik}{4\pi} \int_{-\infty}^{\infty} \int_{-\infty}^{\infty} dxdy \left[1 - e^{-\frac{i}{v_k} \int_{-\infty}^{\infty} dz\, V(x,y,z)} \right] \qquad (E12)$$

Expressing equation (E11) in terms of the forward scattering amplitude yields

$$E(v_k t) = (v_k t)\frac{4\rho\pi}{k} i\, f_e^*(k,k,) + C \qquad (E13)$$

Application of the optical theorem[29] to (E13) produces the desired result,

$$E(v_k t) = (v_k t)(\frac{\rho\sigma_r}{2} + i\, \frac{4\pi\rho}{k} \text{Re}\, f_e(k,k)) + C \qquad (E14)$$

where σ_τ is the helium-helium total cross section and Re $f_e(k,k)$

is the real part of the forward scattering amplitude, both evaluated

in the eikonal approximation. Recalling that C is bounded and

recognizing that it would be rather unusual for σ_τ and Re $f_e(k,k)$

to both be identically zero, equation (E14) shows that for sufficiently

large $v_k t$ the function $E(v_k t)$ will have its value determined by a linear

function of $v_k t$, as stated in Chapter IV.

APPENDIX F

This appendix gives a non-rigorous derivation of the function $P(\omega)$ (refer to Chapter IV, equation (28), which approximately represents the deconvoluted form of $A_4 \exp\{-[(\omega - A_5)/A_6]^4\}$ in equation (22) of Chapter IV, a part of the empirical fit to the scattering data. $P(\omega)$ is obtained by taking the first five terms of the following series

$$\sum_{n=0}^{\infty} \frac{1}{n!} \left(\frac{-\Gamma}{4}\right)^n \frac{d^{2n}}{d\omega^{2n}} A \exp\{-[(\omega - A_5)/A_6]^4\} \qquad (F1)$$

This is in turn based on the claim that

$$f(\omega) = \lim_{\gamma \to 1^+} \sum_{n=0}^{\infty} \frac{1}{n!} \left(\frac{\gamma\Gamma}{4}\right)^n \frac{d^{2n}F(\omega)}{d\omega^{2n}} \qquad (F2)$$

is a solution to

$$F(\omega') = (\pi\Gamma)^{-1/2} \int_{-\infty}^{\infty} d\omega f(\omega) e^{\frac{-(\omega - \omega')^2}{\Gamma}} \qquad (F3)$$

for sufficiently well-behaved functions $F(\omega)$. To demonstrate that equation (F2) is a solution to equation (F3) consider the function

$$R_\gamma(\omega - \omega') = [\pi(1 + \gamma)]^{-1/2} \exp\{-(\omega - \omega')^2/[\Gamma(1 + \gamma)]\} \qquad \text{(F4)}$$

Expand R_γ in a Taylor's series about $\gamma = 0$.

$$R_\gamma(\omega - \omega') = (\pi\Gamma)^{-\frac{1}{2}} \Sigma \frac{\gamma^n}{n!} \frac{\partial^n}{\partial\gamma^n}[(1+\gamma)^{-\frac{1}{2}} \exp\{-(\omega - \omega')^2/[\Gamma(1+\gamma)]\} \qquad \text{(F5)}$$

where in this and subsequent equations n will be used as the summation
index running from 0 to ∞. Note that

$$\frac{\partial}{\partial\gamma}(1 + \gamma)^{-\frac{1}{2}} \exp\{-(\omega - \omega')^2/[\Gamma(1 + \gamma)]\} \qquad \text{(F6)}$$

$$= (\frac{\Gamma}{4}) \frac{\partial^2}{\partial\omega^2}(1 + \gamma)^{-\frac{1}{2}} \exp\{-(\omega-\omega')^2/[\Gamma(1 + \gamma)]\}$$

By an obvious inductive argument

$$\frac{\partial^n}{\partial\gamma^n}(1 + \gamma)^{-\frac{1}{2}} \exp\{-(\omega-\omega')^2/[\Gamma(1 + \gamma)]\} \qquad \text{(F7)}$$

$$= (\frac{\Gamma}{4})^n \frac{\partial^{2n}}{\partial\omega^{2n}}(1 + \gamma)^{-\frac{1}{2}} \exp\{-(\omega-\omega')^2/[\Gamma(1 + \gamma)]\}$$

Therefore

$$R_\gamma(\omega-\omega') = (\pi\Gamma)^{-\frac{1}{2}} \sum \frac{1}{n!} \left(\frac{\gamma\Gamma}{n}\right)^n \frac{\partial^{2n}}{\partial\omega^{2n}} \exp\left[-(\omega-\omega')^2/\Gamma\right] \qquad (F8)$$

As is well known, R_γ forms a delta sequence as γ approaches -1; therefore

$$\delta(\omega-\omega') = \lim_{\gamma\to-1}(\pi\Gamma)^{-\frac{1}{2}} \sum \frac{1}{n!} \left(\frac{\gamma\Gamma}{4}\right)^n \frac{\partial^{2n}}{\partial\omega^{2n}} \exp\left[-(\omega-\omega')^2/\Gamma\right] \qquad (F9)$$

Treating $F(\omega')$ as a known function, write

$$F(\omega') = \int_{-\infty}^{\infty} d\omega \; \delta(\omega-\omega') \; F(\omega) \qquad (F10)$$

Representing the delta function by the delta sequence given in equation (F9) yields

$$F(\omega') = \lim_{\gamma\to-1} (\pi\Gamma)^{-\frac{1}{2}} \int_{-\infty}^{\infty} d\omega \; F(\omega) \qquad (F11)$$

$$x \; \sum \frac{1}{n!} \left(\frac{\gamma\Gamma}{4}\right)^n \frac{\partial^{2n} \exp\left[-(\omega-\omega')^2/\Gamma\right]}{\partial\omega^{2n}}$$

Assuming that $F(\omega)$ is sufficiently well-behaved to allow term-by-term integration, integrate by parts to obtain

$$F(\omega') = \lim_{\gamma \to -1} (\pi\Gamma)^{-1/2} \qquad (F12)$$

$$\times \; \Sigma \; \frac{1}{n!} \left(\frac{\pi\Gamma}{4}\right)^n \int_{-\infty}^{\infty} d\omega' \{\exp\,[-(\omega-\omega')^2/\Gamma]\} \frac{d^{2n}F(\omega)}{d\omega^{2n}}$$

where it is assumed that the boundary terms vanish, i. e.,

$$\lim_{|\omega| \to \infty} e^{-\frac{\omega^2}{\Gamma}} \frac{d^m F(\omega)}{d\omega^m} = 0$$

for all integers m. Again assuming that limit and summation may be interchanged with the integration operation

$$F(\omega') = (\pi\Gamma)^{-1/2} \qquad (F13)$$

$$\times \int_{-\infty}^{\infty} d\omega' \left\{ \lim_{\gamma \to -1} + \Sigma \; \frac{1}{n!} \left(\frac{\gamma\Gamma}{4}\right)^n \frac{d^{2n}F(\omega)}{d\omega^{2n}} \right\} \exp\,[-(\omega-\omega')^2/\Gamma]$$

which demonstrates that the expression in curly brackets,

$$f(\omega) = \lim_{\gamma \to -1} + \Sigma \; \frac{1}{n!} \left(\frac{\gamma\Gamma}{4}\right)^n \frac{d^{2n}F(\omega)}{d\omega^{2n}} \qquad (F14)$$

is a solution to

$$F(\omega') = (\pi\Gamma)^{-1/2} \int_{-\infty}^{\infty} d\omega \; f(\omega) \; \exp\left[-(\omega-\omega')^2/\Gamma\right] \qquad (F15)$$

The above derivation of the form of the deconvoluted function $f(\omega)$ from the experimental data, $F(\omega)$, is clearly not rigorous, since it has not been demonstrated that $F(\omega)$ behaves smoothly enough to validate the interchange of orders of integration, summation, and limit. It is a simple matter to demonstrate that there exist pairs of functions $F(\omega')$ and $f(\omega)$ which simultaneously satisfy equation (F14) and (F15). Rather than try to find the sufficient conditions on $F(\omega')$ and attempt a rigorous proof, the author chose to verify directly that the deconvolution method discussed above suited the use for which it was designed, (refer to the discussion following equation (22) in Chapter IV) - in particular, that

$$P(\omega) = A_4 \sum_{n=0}^{4} \frac{1}{n!} \left(\frac{-\Gamma}{4}\right)^n \frac{d^{2n}}{d\omega^{2n}} e^{-(\omega-A_5)^4/A_6^4} \qquad (F16)$$

is an approximate solution (note that the series is terminated after five terms) to

$$I_3(\omega) \cong (\pi\Gamma)^{-1/2} \int_{-\infty}^{\infty} d\varepsilon \; e^{-(\omega-\varepsilon)^2/\Gamma} P(\varepsilon) \qquad (F17)$$

where $I_3 = A_4 e^{-(\omega-A_5)^4/A_6^4}$ and $\Gamma = (2.1)^2/(4 \ln 2)$ and that the

ω-derivative of equation (F16) is an approximate solution to the

ω-derivative of equation (F17). The adequacy of this approximate

solution is illustrated graphically in Figure 13. Plotted in the

figure as a solid line is the first derivative with respect to energy

loss ω of the term I_3. The corresponding derivative of the

deconvolution of this term, $P(\omega)$, is indicated by the short-dashed

line in the figure. The adequacy of the five term approximation,

$P(\omega)$, is tested by convoluting this $P(\omega)$ with the experimental

Gaussian resolution function, which should then reproduce the term I_3,

or, as well, its ω-derivative. Figure 13 shows that the result for

$dP(\omega)/d\omega$ so convoluted (the long-dashed line in the figure) is

graphically indistinguishable from $dI_3/d\omega$ except in the region
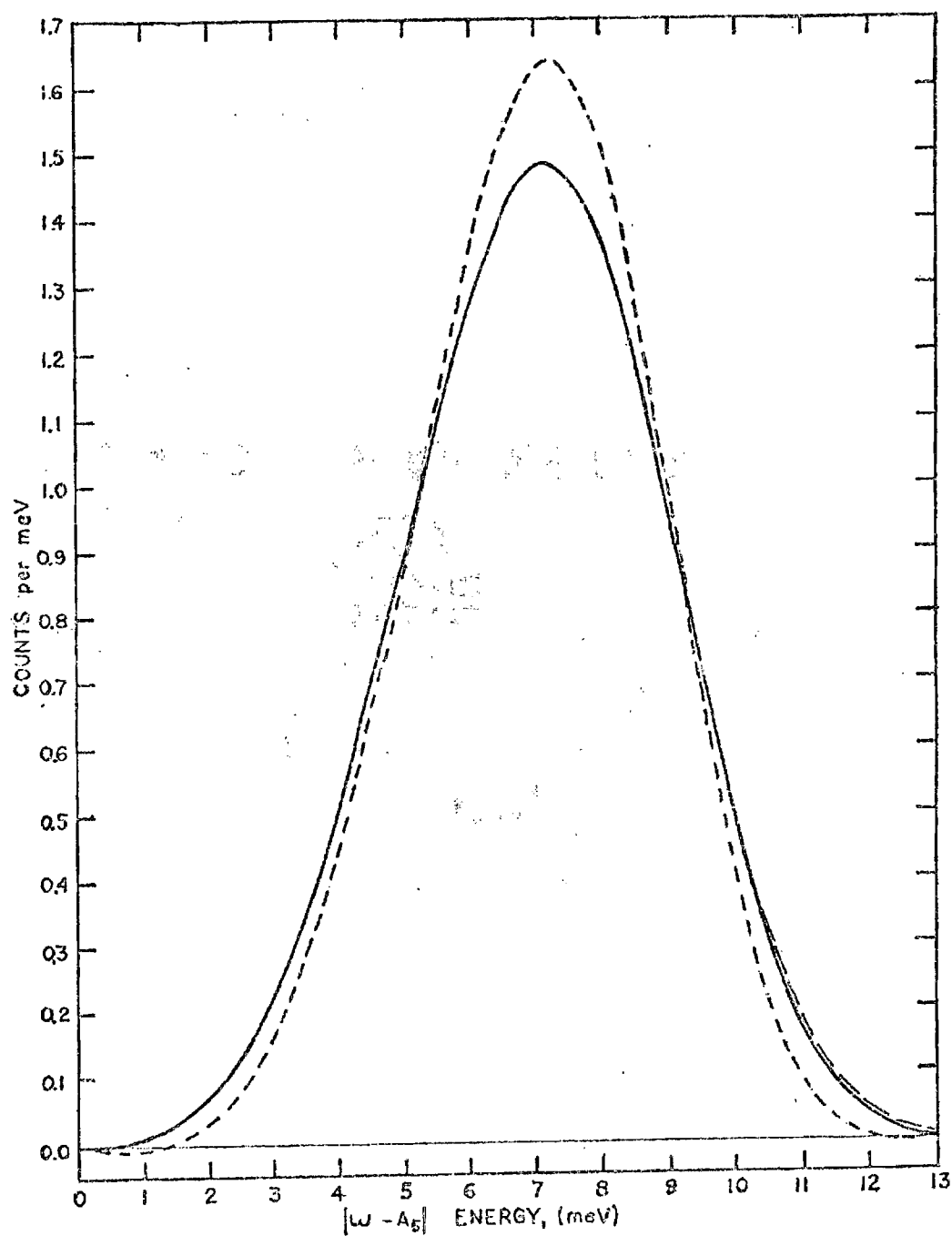
$|\omega-A_5| \gtrsim 10.25$ meV.

Figure 13. Energy Resolution Correction. (The solid line is the ω-derivative of $A_4 \exp-[(\omega-A_5)/A_6]^4$; short-dashed line, ω-derivative of $P(\omega)$ equation (F16); long-dashed line, resolution broadened ω-derivative of $P(\omega)$ where distinguishable from solid line.)

BIBLIOGRAPHY

1. Leighton, R. B., _Principles of Modern Physics_, (McGraw-Hill, New York, 1959).

2. Landau, L. D., Zh. Eksp. Teor. Fiz., 11, 592 (1941); J. Phys. USSR, 11, 91 (1947).

3. McMillan, W. L., Phys. Rev. 138, A442 (1965).

4. Penrose, O., and Onsager, L., Phys. Rev. 104, 576 (1956).

5. Ford, J. and Berlin, T. H., J. Chem. Phys. 27, 931 (1957).

6. Mook, H. A., Scherm, R., and Wilkinson, M. K., Phys. Rev. A (1972).

7. Such experiments were suggested by P. C. Hohenberg and P. M. Platzman, Phys. Rev. 152, 198 (1966).

8. Hove, L. Van, Phys. Rev. 95, 249 (1954).

9. Puff, R. D. and Tenn, J. S., Phys. Rev. A1, 125 (1970).

10. A similar discussion appears in an article by H. A. Gersch and P. N. Smith, Phys. Rev. A4, 281 (1971).

11. Sophisticated methods have been developed to correct scattering data for certain physical limitations in the experimental set-up, such as finite energy and wave-vector resolution.

12. Kerr, W. C., Pathak, K. N., and Singwi, K. S., Phys. Rev. A2, 2416 (1970).

13. Schiff, D. and Verlet, L., Phys. Rev. 160, 208 (1967).

14. Harling, O., K., Phys. Rev. Letters 24, 1046 (1970); Phys. Rev. A3, 1973 (1971).

15. Gersch, H. A. and Smith, P. N., Phys. Rev. A4, 281 (1971).

16. The material in this section is scheduled to appear in Phys. Rev. A (authors: Gersch, H. A. and Rodriguez, L. J.)

17. Gersch, H. A., Rodriguez, L. J., and Smith, P. N., Phys. Rev. A$\underline{5}$, 1547 (1972).

18. This identity was suggested by Q. Bui Duy.

19. See H. Cramer, Mathematical Methods of Statistics (Princeton U. P., Princeton, N. J., 1951), p. 186. Cumulant expansions for c-number products in scattering theory have been previously utilized by R.J. Glauber, Lectures in Theoretical Physics, edited by W. E. Brittin and L. G. Dunham (Interscience, New York, 1959), Vol. 1. Cumulant expansions have also been applied to time-ordered operators, for example, see R. Kubo, in Fluctuation, Relaxation, and Resonance in Magnetic Systems, edited by D. ter Harr (Oliver and Boyd, Edinburgh, Scotland, 1962).

20. Later calculations will be performed using the Lennard-Jones Potential $V(r) = 4\epsilon[(\sigma/r)^{12} - (\sigma/r)^6]$, where σ and ϵ are constants. The claim that $R(k,t)$ approaches unity for all times for sufficiently large k may not be valid for this potential because of the singularity of the potential at $r = 0$. If desired, one could avoid this problem by choosing a bounded potential to represent the helium-helium interaction. In the author's opinion, one is relieved of the necessity of resolving this point by the observation that the potential $V(r)$ becomes physically meaningless for sufficiently small r. For practical purposes one only needs to be convinced that for sufficiently large k, $R(k,t)$ will remain close to unity for large time interval about $t = 0$. The Fourier transform $R(k, v_k\Omega - \vec{v}_k\cdot\vec{p})$ will then have a narrow width. When the width of $R(k, v_k\Omega - \vec{v}_k\cdot\vec{p})$ becomes narrow compared to the width of n_p, $R(k, v_k\Omega - \vec{v}_k\cdot\vec{p})$ may be replaced by a delta function to some reasonable approximation (assuming R is not pathological).

21. The material in this chapter has been prepared for publication (authors: L. J. Rodriguez, H. A. Gersch, and H. A. Mook).

22. Numerical values tabulated in Appendix B.

23. Feltgen, R., Pauly, H., Torello, F., and Vehmeyer, H., Phys. Rev. Letters $\underline{30}$, 820 (1973).

24. An attempt at including effects of the attractive part of the helium-helium potential in $f(r)$ is reported by R. D. Murphy, Phys. Rev. A$\underline{5}$, 331 (1972). He used the form $f(r)=\exp[-(a/r)^n \pm (a/r)^m]$ where the plus sign in front of the second term in the exponential would correspond to attractive interactions. He finds that the negative sign yields superior results. However, using the same range parameter a for both repulsive and attractive terms is highly artificial and is not strong evidence against the appearance of an effect of the attractive part of the potential in $f(r)$.

25. The helium number density has been taken to be .022 atoms per $\overset{\circ}{A}{}^3$.

26. The values of $R(k, v_k\Omega)$ were obtained by Fourier transforming an approximation to $R(k,t) = \exp[-E(v_k t)]$. The approximation used for $R(k,t)$ was obtained by linear interpolation of $E(v_k t)$ between the tabulated values (refer to Table 2) and a linear extrapolation of $E(v_k t)$ beyond the largest tabulated value of $v_k t$.

27. The condensate fraction was taken to be .11 at 1.2°K. This was done to facilitate comparison with the results of a Monte Carlo calculation, Reference 3. The condensate fraction was taken as identically zero at a helium temperature of 4.2°K.

28. The experimental data is proportional to the dynamic structure factor $S(k,\omega)$ broadened by an experimental resolution function with a full width at half maximum of approximately 2.1 meV. The data at 4.2°K has been corrected for the difference in the helium liquid density at 1.2°K and 4.2°K.

29. Schiff, L. I., Quantum Mechanics, Third Edition, McGraw-Hill, 1968.

VITA

Leonard Julius Rodriguez was born on December 15, 1943 in Utica, New York. In 1962 he graduated from Chamberlain High School in Tampa, Florida. He received the degree of Bachelor of Science in Physics from the Georgia Institute of Technology in 1966. While employed by Hamilton Standard Division of United Aircraft Corporation, he completed the requirements for a Master of Science degree in 1969 at Trinity College, Hartford, Connecticut.

He married the former Jean Moss of New York City on September 4, 1965. They have two children, Jean Caroline and Timothy Wade.